The hypothalamus as a hub for putative SARS-CoV-2 brain infection

Sreekala Nampoothiri[1,2], Florent Sauve[1,2#], Gaëtan Ternier[1,2#], Daniela Fernandois[1,2#], Caio Coelho[1,2], Monica Imbernon[1,2], Eleonora Deligia[1,2], Romain Perbet[1], Vincent Florent[1,2,3], Marc Baroncini[1,2], Florence Pasquier[1,4], François Trottein[5], Claude-Alain Maurage[1,2], Virginie Mattot[1,2‡], Paolo Giacobini[1,2‡], S. Rasika[1,2‡]*, Vincent Prevot[1,2‡]*

[1] Univ. Lille, Inserm, CHU Lille, Lille Neuroscience & Cognition, DistAlz, UMR-S 1172, Lille, France
[2] Laboratory of Development and Plasticity of the Neuroendocrine Brain, FHU 1000 days for health, EGID, School of Medicine, Lille, France
[3] Nutrition, Arras General Hospital, Arras, France
[4] Centre mémoire ressources et recherche, CHU Lille, LiCEND, Lille, France
[5] Univ. Lille, CNRS, INSERM, CHU Lille, Institut Pasteur de Lille, U1019 - UMR 8204 - CIIL - Center for Infection and Immunity of Lille (CIIL), Lille, France.

# These authors contributed equally to this work.

‡ These authors directed this work

*Correspondence to: vincent.prevot@inserm.fr and sowmyalakshmi.rasika@inserm.fr

Short title: **Covid-19: the hypothalamic hypothesis**

Abstract

Most patients with COVID-19, caused by severe acute respiratory syndrome coronavirus 2 (SARS-CoV-2), display neurological symptoms, and respiratory failure in certain cases could be of extra-pulmonary origin. With reports detecting SARS-CoV-2 in some post-mortem patient brains, the routes, targets and consequences of brain infection merit investigation. Hypothalamic neural circuits play key roles in sex differences, diabetes, hypertension, obesity and aging, all risk factors for severe COVID-19, besides being connected to brainstem cardiorespiratory centers. Here, human brain gene-expression analyses reveal that the hypothalamus and associated regions express angiotensin-converting enzyme 2 and transmembrane proteinase, serine 2, which mediate SARS-CoV-2 cellular entry, in correlation with several genes or pathways involved in physiological functions or viral pathogenesis. Immunolabeling in human and animal brains suggests that the hypothalamus could be central to SARS-CoV-2 brain invasion through multiple routes, and that sex hormones and metabolic diseases influence brain susceptibility.

Main text

Increasing evidence is coming to light associating SARS-CoV-2 infection with a wide range of neurological symptoms (headaches, dizziness, nausea, loss of consciousness, seizures, encephalitis etc.) ((*1-5*), reviewed in (*6-9*), as well as anosmia or ageusia in more than two-thirds of patients (*10, 11*). Additionally, a large number of COVID-19 patients with severe disease do not respond well to artificial ventilation or display a phenomenon known as "silent hypoxia", where low blood oxygen levels fail to trigger the appropriate physiological response (*12*), suggesting an extra-pulmonary component to respiratory dysfunction, and cardiorespiratory function and fluid homeostasis are themselves subject to central nervous system (CNS) control. However, despite emerging reports of the post-mortem detection of the virus in the cerebrospinal fluid (CSF) (*13, 14*) or brain parenchyma of patients (*15*), very little is known so far about how and under what circumstances SARS-CoV-2 infects the brain or nervous system.

While the possibility of CNS infection has been largely underestimated due to the common view that angiotensin converting enzyme 2 (ACE2), the only confirmed cellular receptor for SARS-CoV-2 so far (*16-19*), is absent or expressed only at very low levels in the brain (*20, 21*)), and that too exclusively in vascular cells (He et al., bioRxiv 2020; doi: https://doi.org/10.1101/2020.05.11.088500) the majority of these studies have focused on the cerebral cortex, ignoring the fact that other regions of the brain, notably the hypothalamus, are rich in ACE2, at least in animals (*22*) (*23*). Indeed, the highly related SARS-CoV has been observed by several investigators in post-mortem human brain tissue, including the hypothalamus (*24-26*). Furthermore, altered labeling for several hormones in post-mortem pituitary tissue (*27*) as well as long-term neuroendocrine deficits in some survivors of SARS-CoV infection (*28*) strongly support the notion of the hypothalamus as a target of viral infection. Intriguingly, most major risk factors for severe COVID-19 (male sex, age, obesity, hypertension, diabetes) ((*29-32*); reviewed by (*33*) (*31, 34-36*)) could be mediated by normal or dysfunctional hypothalamic neural networks that regulate a variety of physiological processes: sexual differentiation and gonadal hormone production, energy homeostasis, fluid homeostasis/osmoregulation and even ageing (*37-40*). The hypothalamus is also directly linked to other parts of the CNS involved in functions affected in COVID-19 patients, including several

brainstem nuclei that control fluid homeostasis, cardiac function and respiration, as well as regions implicated in the perception or integration of odor and taste such as the olfactory bulbs and presumptive vomeronasal neurons, the entorhinal and piriform cortices, the insula, amygdala, and thalamus (*37, 39, 41-44*). This is of particular interest as the loss of the sense of smell or taste in the majority of COVID-19 patients suggests that the virus could invade the brain through sensory receptors.

Here, we investigated the susceptibility of the hypothalamus and related brain regions to SARS-CoV-2 infection by analyzing the expression of ACE2 and the transmembrane proteinase, serine 2 (TMPRSS2), which cleaves the SARS-CoV-2 spike (S) protein, thus enabling it to be internalized, from existing data from the Allen Human Brain Atlas (AHBA) (*45*). We also used network analysis and pathway enrichment tools to determine which genes and cellular, molecular or disease processes were correlated with this susceptibility, and whether they were similar to differentially expressed genes in the respiratory epithelium of COVID-19 patients (*46*). Finally, we confirmed our hypothesis by immunolabeling for ACE2, TMPRSS2 and other genes of interest in the hypothalamus of mice, hamsters and control human brains.

ACE2 and TMPRSS2 are expressed in the human hypothalamus and connected brain regions

The AHBA, comprising 3702 anatomical brain regions from six donors (five males and one female, mean age 42, range 24–57 years), contains microarray gene expression data for >62,000 gene probes, including ACE2 and TMPRSS2. We thus used the atlas to first investigate the occurrence of ACE2 and TMPRSS2 in a number of hypothalamic nuclei and connected regions involved in regulating olfaction, gustation or cardiorespiratory function: the insula, the amygdala, the paraventricular nucleus of the thalamus, the pons and the myelencephalon (**Fig. 1a**). The frontal lobe and cerebellar cortex as well as the choroid plexus were included for comparison. The olfactory bulbs and some brainstem regions are unfortunately not represented in the AHBA. We selected probes *CUST_16267_PI416261804* for ACE2 and *A_23_P29067* for TMPRSS2 based on their maximum variance across all samples. Using normalized log2 intensity values to calculate the median expression level and nonparametric missing value imputation for regions where the number or quality of the samples was inadequate (see Methods), we observed that the expression levels of both genes varied widely across and within the brain regions studied (**Fig. 1b, Suppl. Table 1, Suppl. Movie**). Of note, as expected from previous studies (*47*) (He et al., bioRxiv, 2020; https://doi.org/10.1101/2020.05.11.088500), ACE2 expression levels in the cerebral cortex (frontal lobe, insula) and cerebellar cortex were relatively low, while the paraventricular nucleus of the hypothalamus (PVH) displayed the highest ACE2 levels among hypothalamic nuclei, in keeping with its role in fluid homeostasis through the renin-angiotensin system (*48*). Surprisingly, the choroid plexus displayed extremely high ACE2 levels. TMPRSS2 was present in all the areas studied, and its levels were, on the whole, higher than those of ACE2. Relatively high levels of both ACE2 and TMPRSS2 were found in a number of regions, including the PVH and several areas of the brainstem, indicating that they are potential targets of SARS-CoV-2.

Genes correlated with ACE2/TMPRSS2 and SARS-CoV-2 infection in key brain structures

We next proceeded to identify genes whose expression was positively or negatively correlated with the selected ACE2 or TMPRSS2 probes, using their normalized log2intensity gene expression values and the *Find Correlates* option in the AHBA, for 5 regions of interest – the insula, the amygdala, the

hypothalamus, the parabrachial nucleus in the pons, and the myelencephalon (**Fig. 2a**). Probes with zero entrez-id were eliminated, and if multiple probes represented a single gene, the one with the lowest adjusted p value was retained. The paraventricular thalamic nucleus was sampled in only three brains in the AHBA, and had to be excluded following analysis of Pearson's correlation coefficients. The pontine tegmentum and basal pons were also eliminated from further analysis because the diversity and number of regions yielded results that were hard to interpret. However, the parabrachial nucleus of the pons, which was comparable to the diencephalic and telencephalic regions analyzed and key to the functions studied here, was retained. Out of several thousand genes whose expression was found to be correlated with ACE2 or TMRPSS2 in the 5 regions (**Fig. 2b,c**), we identified 2786 with a Pearson's coefficient (r value) between -0.3 and 0.3, a p value of < 0.01 and a false discovery rate (FDR) < 0.25 for ACE2, and 5369 for TMPRSS2, in the hypothalamus alone (**Suppl. Table 2**). Of these, 1985 were correlated with both ACE2 and TMPRSS2, making them possible candidates of interest for infectious mechanisms or the host cell response. According to the GSEA User Guide, an FDR of <0.25 is reasonable in an exploratory setting, where the aim is to find candidate hypotheses, and where a more stringent FDR cutoff may lead to potentially significant results being overlooked because of the lack of coherence in most expression datasets (see also (*49*). In order to draw parallels between SARS-CoV-2 infection of the respiratory epithelium and a putative brain infection, we further cross-checked our genes against those found to be differentially expressed in the lungs of COVID-19 patients as compared to healthy individuals (*46*). A total of 140 genes with a variety of known functions were both correlated with ACE2 and TMPRSS2 expression in the hypothalamus according to the AHBA and differentially expressed in COVID-19 patients (**Fig. 2d, Suppl. Table 3**). The expression of a further 62 and 329 genes, respectively, was correlated with only ACE2 or only TMPRSS2.

ACE2/TMPRSS2-correlated genes are involved in functional networks of interest

To obtain an idea of the possible mechanisms at play if certain ACE2- or TMPRSS2-correlated genes were to be involved in SARS-CoV-2 pathogenesis, we then performed enrichment analyses on these genes (-0.3 < r < 0.3; fdr < 0.25) for KEGG pathways using the Clusterprofiler package in R. The KEGG pathway database, which is manually curated, can be used to identify genes that are known to be implicated in a number of molecular processes and networks in the following categories: metabolism, genetic information processing, environmental information processing, cellular processes, organismal systems, human diseases and drug development. Pathway enrichment and selection yielded a number of important functions and interactions among the genes correlated with ACE2 and/or TMPRSS for each brain region analyzed (**Fig. 3a,b**). With regard to ACE2-correlated genes, gene enrichment in the myelencephalon and pons revealed a very large number of KEGG pathways with a small number of significantly correlated genes, perhaps due to the diverse peripheral inputs they integrate. For this reason, only pathways with a q value of < 0.05 are shown (**Fig. 3a**). In contrast, the insula yielded 2 enriched pathways for ACE2-correlated genes, and the amygdala 4. The pathways with the most correlated genes were both localized in the hypothalamus, and were for "olfactory transduction" (due to a very large number of OR olfactory receptor genes) and "neuroactive ligand-receptor interaction", in keeping with the variety of neuropeptides and neurotransmitters produced by hypothalamic neural networks.

KEGG pathway enrichment of TMPRSS2-correlated genes (**Fig. 3b**) revealed very few pathways in the same q value range used for ACE2. We therefore applied the original exploratory cutoff of q < 0.25

(the point of the exercise being to identify likely patterns rather than any single significantly correlated pathway; see Methods). In contrast to ACE2-correlated genes, under these conditions, pathway enrichment for TMPRSS2-correlated genes revealed a lower number of pathways in the hypothalamus, myelencephalon and pons, but a higher number in the insula and amygdala. Here too, the largest pathways were for "neuroactive ligand-receptor interaction" and "olfactory transduction" in the hypothalamus, suggesting that these two pathways could be of unusual importance when taken together with ACE2 and TMPRSS2, and providing some support for our focus on anosmia and neuroendocrine function in SARS-CoV-2 pathogenesis. In addition to these, other common enriched pathways between ACE2- and TMPRSS2-correlated genes were those for "taste transduction", "cAMP signaling", "Cushing syndrome" and "hematopoietic cell lineage". However the latter two were not enriched in the hypothalamus with regard to TMPRSS2-correlated genes. While this is not in itself an indication that genes involved in these networks do not play important roles in SARS-CoV-2 susceptibility or pathogenesis, we chose not to analyze them further in order to keep our study manageable.

We additionally performed enrichment for gene ontology (GO) terms, which are also manually curated and classify genes in identified pathways among the following categories: "biological processes", "cellular components" and "molecular function" (**Suppl. Table 4,5**).

Functionally connected brain regions express common ACE2- and TMPRSS2-correlated genes and pathways

While, pathway enrichment allows likely functional links to be pinpointed by identifying groups of genes that are jointly correlated, the relationship between pathways and individual genes that might connect them or that are similarly correlated in several functionally linked areas could also be informative from the point of view of the pathophysiological mechanisms involved. We therefore built gene networks based on the pathways identified above for ACE2- (**Suppl. Fig. 1-5**) and TMPRSS2-correlated genes (**Suppl. Fig. 6-10**) in each of the 5 regions. Interestingly, since the gene sets comprising each pathway are manually curated, this exercise allowed us to identify certain genes that we believed to be of interest for more than one function or pathway even though they did not appear in that pathway in the enrichment analysis. Next, we analyzed the four pathways identified above that were correlated with both ACE2 and TMPRSS2 in the hypothalamus as well as other connected regions: "neuroactive ligand-receptor interaction" (**Fig. 4a,b**), "olfactory transduction" (**Fig. 4c,d**), "taste transduction" (**Fig. 4e,f**) and "cAMP signaling" (**Fig. 4g,h**). For each of these networks, a number of genes that were correlated with ACE2 and/or TMPRSS2 were also expressed as part of the same or linked pathways across multiple brain areas, suggesting that they could be involved in common physiological functions or signaling mechanisms involving ACE2 or TMPRSS2 in these areas. In addition, both among these common genes and genes that were only present in a single region, we found several whose expression was also altered by SARS-CoV-2 infection in the lung (*46*), suggesting that regardless of any tissue-specific functional pathways identified, these genes could be involved in susceptibility or response to the virus. **Table 1** highlights these likely important genes along with what is known of their function or potential role in SARS-CoV-2 pathogenesis. Intriguingly, this list included the formyl peptide receptor FPR2 (also known as ALX or FPRL1), a molecule that is closely related to vomeronasal receptors (*50*) but that detects peptides of pathogenic or mitochondrial origin and has either inflammation-resolving or pro-inflammatory actions (*51*).

ACE2 and TMPRSS2 are present in olfactory neurons and hypothalamic neurons and tanycytes in humans

To validate the relevance of our gene expression and network analysis results to human patients, we performed immunolabeling for ACE2, TMPRSS2 as well as FPR2 using available antibodies on sections of control adult human brains and fetal heads. In the adult brain, the choroid plexus was strongly positive and served as a positive control for both ACE2 and TMPRSS2 (**Fig. 5a**). In the PVH parenchyma, in keeping with the involvement of this region in fluid homeostasis, ACE2 was present in cells with a neuronal morphology, as well as a few capillary walls (**Fig. 5b**). Interestingly, it was colocalized with FPR2, which we identified in several brain regions above as being correlated with ACE2 and TMPRSS2 in addition to being differentially expressed in COVID-19 patient lungs, in the neurons. Some FPR2-positive fibers or cell bodies, possibly glial, were visible close to the ventricular wall, but did not appear to be colocalized with fibers positive for vimentin (**Fig. 5c**), a marker in the hypothalamus for specialized ependymoglial cells called tanycytes. Lower down the ventricular wall, at the level of the arcuate nucleus of the hypothalamus (ARH) and median eminence (ME), a circumventricular organ (CVO) at which the traditional blood-brain barrier has been replaced by a fenestrated endothelium and a barrier consisting of tanycytes, light ACE2 labeling was seen in a few tanycytic processes radiating from their cell bodies in the ventricular wall (**Fig. 5d**). Interestingly, ACE2 in these processes colocalized with TMPRSS2, suggesting that the machinery for SARS-CoV-2 infection is present in these cells. Some capillary walls were also positive for ACE2 as expected, as were some cells with a neuronal morphology (**Fig. 5d**). TMPRSS2 was strongly colocalized with vimentin-positive tanycytic processes in the ARH and ME at both the ventricular wall and the pial surfaces (**Fig. 5e,f**). Combined with the presence of ACE2 in tanycytes themselves or other adjacent cells, even if this is only at low levels in the absence of risk factors, the presence of TMPRSS2 may render these cells susceptible to SARS-CoV-2 infection.

In order to investigate the olfactory route, given the absence of olfactory bulb data in the AHBA, we also performed ACE2 and TMPRSS2 labeling in whole head sections of human embryos at gestational week (GW) 11 (**Fig. 5g**) or 14 (**Fig. 5j**). Both ACE2 (**Fig. 5h**) and TMPRSS2 (**Fig. 5i**) were strongly colocalized along the TAG-1 (or contactin 2, CNTN2)-immunoreactive olfactory/vomeronasal axons that start targeting the olfactory bulbs at those developmental stages. Notably, at GW11, all cells in the olfactory epithelium (OE) were positive for ACE2 and for TMPRSS2 (**Fig. 5h,i**), and both proteins were strongly expressed in the developing olfactory bulb (OB) (**Fig. 5h,i**). At GW14, when the neuronal layer of the OE and the embryonic vomeronasal organ (VNO) were further developed, strong immunolabeling for both ACE2 and TMPRSS2 was observed in the apical layer of both the OE and the VNO, in addition to the olfactory nerve (ON), most likely corresponding to the olfactory and the vomeronasal sensory neurons, respectively (**Fig. 5k,l,m**). FPR2 did not appear to be present in these sections, and is not known to occur in the nose.

ACE2, TMPRSS2 and FPR2 are expressed in the hamster and mouse hypothalamus and are upregulated by high-fat diet and ovariectomy

In order to validate our gene expression data in terms of protein expression and localization, we next performed immunofluorescence labeling for ACE2, TMPRSS2 and FPR2 in brain sections from male hamsters, a model that is susceptible to SARS-CoV-2 infection even without genetic modification due to their higher homology with human ACE2 than mice (*52*). Using the same antibody to human ACE2

that we used in the human brain sections, we found clear confirmation of the presence of ACE2 in the processes of a large number of vimentin-positive tanycytes spanning the hypothalamic parenchyma from the wall of the third ventricle, where their cell bodies are located, to the external surface, where their endfeet are in contact with the capillary bed. In addition to the numerous ME/ARH tanycytes, a few dorsal tanycytes, further up along the wall of the 3rd ventricle, also expressed abundant ACE2 from their cell bodies and processes (**Fig. 6a**). In addition, the same tanycytes also expressed TMPRSS2 (**Fig. 6a**), again underscoring the fact that tanycytes could provide an entry mechanism for the virus into the brain through either the hematogenous or the CSF route.

Despite the usefulness of the hamster as a model for SARS-CoV-2 infection, pathophysiological mechanisms are easier to elucidate and validate in mice due to the wealth of literature. Out of curiosity with regard to the increased risk of SARS-CoV-2 infection in certain individuals, we therefore next evaluated the effect on ACE2, TMPRSS2 and FPR2 of a standard or high-fat diet (HFD), which induces obesity, and the effect of the gonadal steroid estrogen, given the difference in the risk of developing severe COVID-19 in men and women.

In the brain of mice fed normally, we first validated an antibody to mouse ACE2. Immunofluorescence using this antibody in most parts of the adult mouse brain appeared to be limited to cells of the capillary walls – pericytes or endothelial cells (**Fig. 6b**) – as previously described (*47*) (He et al., bioRxiv, 2020; https://doi.org/10.1101/2020.05.11.088500). However, in the choroid plexus, where ACE2 levels were among the highest seen in our gene expression analysis of human brains (**Fig. 1b**), ACE2 immunofluorescence appeared to be present as an apical cap on these cells (**Fig. 6c**), confirming our observations in the human cortex and choroid plexus. In contrast, in the PVH of male mice with a normal diet (**Fig. 6d, left panels**), ACE2 appeared to be present in scattered neurons in addition to vascular cells, as seen in the human brain with regard to this nucleus involved in the renin-angiotensin system. Intriguingly, however, in the ME of male (**Fig. 6e, left panels**) and female mice (**Fig. 6f, left panels**), tanycytes, in addition to vascular cells, showed the most labeling. Both the cell bodies of tanycytes at the wall of the third ventricle in the ME and the adjacent ARH, and their processes extending towards the external capillary bed were labeled for ACE2, as was the pars tuberalis, a highly vascularized zone under the ME. TMPRSS2 labeling was also found predominantly in tanycytic cell bodies and processes in the ARH and ME, but was found in astrocyte-like cells at the ventricular wall adjacent to the PVH and some microglia-like cells in the PVH parenchyma (**Fig. 6d,e,f, left panels**). Surprisingly, FPR2 was found to be strongly expressed in cells with an astrocytic morphology along the ventricular wall at the PVH, where it sometimes colocalized with TMPRSS2, and in both tanycytic cell bodies and processes along the ventricle and microglia-like cells in the ARH and ME (**Fig. 6d,e,g**), where two neuronal populations, expressing NPY and POMC, that control energy metabolism reside (*46*).

Next, we examined the same three markers in male mice given a HFD for 9 weeks to induce obesity (**Fig. 6d,e, right panels**) as well as in ovariectomized (OVX) female mice (**Fig. 6f, right panels**). Strikingly, in the male HFD mice there was a strong upregulation of ACE2 in vascular cells in the ARH, while at the same time, ACE2 immunolabeling was reduced in the cell bodies of ME/ARH tanycytes and completely abolished in their processes (**Fig. 6e, right panels**). However, apical labeling like that seen in the choroid plexus appeared at the level of the tanycytes in the dorsal ARH, while the pars tuberalis was less strongly labeled (**Fig. 6e, right panels**). ACE2 also increased in the PVH with the HFD, but the pattern and cell types labeled did not change (**Fig. 6d, right panels**). TMPRSS2 also

increased with HFD in both the microglia-like cells of the PVH and the cell bodies of tanycytes in the ME/ARH, but to a less remarkable extent (**Fig. 6d,e, right panels**). Importantly OVX female mice displayed the same changes in ACE2 and TMPRSS2 immunolabeling as male HFD mice (**Fig. 6f**), i.e. ACE2, present in ME/ARH tanycytic cell bodies and processes under normal conditions, disappeared in OVX females to be replaced by increased labeling at the apical poles of more dorsal tanycytes and vascular cells. Labeling for TMPRSS2 similarly mimicked the changes seen in HFD. On the other hand, FPR2 immunolabeling in HFD mice showed a dramatic increase in the number and spatial extent of astrocyte-like cells along the ventricular wall and in the PVH parenchyma, as well as in tanycytic cell bodies lining the ventricle and processes reaching the external capillary bed in the ARH and ME; in addition, there was an increase in the microglia-like labeling in the latter, in keeping with microglial activation during an inflammatory state (**Fig. 5c,d, right panels**) (*53*). However, these observations regarding FPR2 were not evident in OVX females.

Finally, given the diversity of these results, we next used fluorescence-associated cell sorting (FACS) to sort cells from the median eminence of mice expressing tdTomato selectively in tanycytes (*54*) (**Fig. 6h**). In the resulting Tomato-positive and Tomato negative cells, we performed RTqPCR for ACE2, TMPRSS2, FPR2 and the tanycytic marker vimentin (bottom panel) to confirm that Tomato-positive and –negative sorted cells were tanycytes and non-tanycytes respectively. While ACE2 was present in both populations as indicated by immunolabeling experiments (**Fig. 6e,f**), TMPRSS2 was expressed almost exclusively in tanycytes in this region and FPR2 was expressed in both tanycytes and non-tanycytic cells. These results strongly suggest that ACE2 and TMPRSS2 could form part of a pro-inflammatory pathway mediated by differential FPR2 expression, through which risk factors such as metabolic diseases and male sex (or the absence of female sex) could increase susceptibility to and outcome of SARS-CoV-2 infection by altering the pattern of ACE2 expression in vulnerable hypothalamic circuits.

Discussion

Six months and several thousand papers and preprints after the beginning of the pandemic, if there is one thing we have learnt about SARS-CoV-2, it is that almost every assumption that has been made about the virus has been wrong. Although viral pneumonia is still the principal symptom in severely ill patients and a large number of complications affecting a variety of organs and physiological processes stem from two accompanying phenomena – the "cytokine storm" and a prothrombotic state (*30, 31, 55-57*), other tissues, notably the gut, are also directly susceptible to infection (*58*). While our study may seem at first sight to resemble the parable of the blind men and the elephant, we consider the possibility that SARS-CoV-2 infiltrates the brain, and specifically the hypothalamus, with functional consequences to disease progression and outcome, to be more in the nature of the elephant in the room.

The idea that SARS-CoV-2 could infect the brain, in particular through an olfactory route, has been proposed by other authors (*9, 59, 60*), both in light of the observation of anosmia in COVID-19 patients and from experimental studies on SARS-CoV, which uses the same receptor and protease as SARS-CoV-2. In these previous studies, SARS-CoV administered intranasally in transgenic mice expressing human ACE2 directly entered the brain through the OE and OBs, and was found at high concentrations in the hypothalamus and brainstem within a matter of days (*61-64*). Furthermore, it

was not the occurrence of viral pneumonia per se but brain infection that determined mortality (*64*). Additionally, a recent MRI study has revealed changes to the OBs of a patient with anosmia (*65*), although this could be secondary to changes in the epithelium rather than due to viral invasion. While it has been proposed that it is the sustentacular cells of the OE or secretory cells that express ACE2 and are infected by SARS-CoV-2 and not olfactory sensory neurons themselves (*66*), in our study, at least in the human embryo, olfactory and vomeronasal sensory neurons do appear to express both ACE2 and TMPRSS2 at high levels. In addition, even if this neuronal expression were limited to the developmental stage, structural analyses of the S protein indicate the possibility of alternative receptors, notably sialic acid or the integrins (*67, 68*), both of which abound in the adult OBs and could allow the virus to make its way to the hypothalamus or other target tissues. It should also be remembered that the ON and vomeronasal nerve also serve as a scaffold to guide gonadotropin-releasing hormone (GnRH) neurons from the nose to the hypothalamus during development (*69*), and that these GnRH neurons persist as a continuum along this route into adulthood, firmly and directly connecting the olfactory route to the hypothalamus. In addition, the inclusion of an extra loop at the protease cleavage site of the S protein of SARS-CoV-2 makes it theoretically possible that proteases other than TMPRSS2, notably cathepsins B or L, could cleave it or alter its fusion properties (*70*), further expanding the range of putative susceptible cells both in the CNS and elsewhere. So long as the activating protease is not very far removed from the host cell expressing the receptor, there is no need for colocalization of the two molecules on the same cell, as *trans* activation of the virus is a possibility (*71*).

Other routes for brain infection have also been proposed, notably through other peripheral nerves from sensory or visceral organs that are important targets of infection, or a hematogenous route. Although one criticism of the latter proposition has been that the virus is rarely detected in the blood of patients, a closer look at the literature reveals that the virus is not only detected by PCR in a variable percentage of infected individuals, but that the chances of detecting it are higher in severely ill patients (see for example (*72*)), either because of higher viral load in these patients or because endothelial barriers in peripheral organs break down in these patients, allowing the virus to enter the bloodstream. Once in the bloodstream, the virus could access the brain through a number of routes, for example, through the leaky endothelial barrier in the other direction, given the expression of ACE2 by pericytes. The virus could also enter the brain through the fenestrated capillaries of the CVOs, which include the hypothalamic ME and organum vasculosum of the lamina terminalis, as well as the subfornical organ and area postrema (*73, 74*), all of which play key roles in either the risk factors or the physiological functions targeted by SARS-CoV-2. Indeed, our immunolabeling experiments in both animals and humans show that ACE2, while low, is present in ME and ARH tanycytes, whose endfeet contact these fenestrations, in addition to vessels themselves. In addition, viral particles could enter the CSF through the choroid plexus, which we show to be rich in both ACE2 and TMPRSS2, and thereby access other brain regions, including hypothalamic nuclei bordering the third ventricle, where we once more observe ACE2-positive tanycytic cell bodies. Finally, as can be seen by immunolabeling in the hypothalamus of HFD-fed or ovariectomized mice, certain risk factors such as obesity or certain gonadal hormones could increase ACE2 levels or alter the pattern of its expression, and therefore the susceptibility to infection in specific cell types or by specific routes.

Regardless of the entry route, once in the brain, the virus could infect a number of different regions through the same transsynaptic or other mechanism likely to be used in the olfactory route or by diffusion through the CSF. However, given the high incidence of anosmia and ageusia in addition to

respiratory dysfunction, and the relationship between hypothalamic neural circuits and the large majority of risk factors for severe COVID-19, we chose to focus our gene expression analysis on those regions implicated in these functions. Surprisingly, among the four most ubiquitous enriched pathways for genes correlated, positively or negatively, with ACE2 or TMPRSS2, we found the pathways for olfactory and taste transduction, with a very large number of OR and TAS genes expressed in the hypothalamus, amygdala and insula. Both OR and TAS genes, members of the vast family of G protein-coupled receptors (GPCRs) have previously been found in "ectopic" locations, within and outside the brain, and appear to play other roles than as receptors for odor or taste (see for review, (*75*). Taste receptors in particular are interesting because they could be involved in the sensing of peripheral metabolites by hypothalamic tanycytes, and could thus be over- or under-expressed in disorders like obesity or diabetes, which are risk factors for severe COVID-19. In addition, they are expressed in the airway epithelium and mediate both the host response to pathogens and viral susceptibility (*76, 77*), even though they were not shown to be particularly enriched in COVID-19 lung biopsy data(*46*).

Our network analysis and immunolabeling studies also unexpectedly revealed another GPCR, the inflammatory mediator FPR2, as playing a key role in the potential viral infection of the brain through ACE2. While FPR2 can mediate certain anti-inflammatory effects, it appears to be involved in the replication of double-stranded viral RNA, an important step in the propagation of RNA viruses (*78, 79*). In addition, ACE2 expression was positively correlated with FPR2 expression in our gene expression analysis from the AHBA, and both ACE2 and FPR2 were found to be higher in HFD-fed animals. This is of interest as the hypothalamus, which harbors various neuronal populations that express neuronal nitric oxide synthase (nNOS) or that control feeding and energy expenditure in response to metabolic signals from the periphery (*80*) (*81, 82*), exhibits inflammation in case of obesity (*83*), and nitric oxide has itself been shown to inhibit the replication of SARS-CoV (*84*). Additionally, the deletion of FPR2 in mice alleviates HFD-induced obesity, insulin resistance and other adverse metabolic indicators by suppressing pro-inflammatory mechanisms in the periphery (*85*), suggesting that it could potentially exacerbate the effects of SARS-CoV-2 infection in patients with metabolic diseases. Paradoxically, we have recently shown that anorexia induced by systemic proinflammatory cytokines, such as in severe viral infection, is also mediated by hypothalamic tanycytes, through the IKK subunit Nemo or IKBKG (*86*); IKBKG is also highlighted by our gene expression data and is differentially expressed in the lung of COVID-19 patients (*46*). Additionally, the changes we observed in ACE2 expression in the hypothalamus, and especially in the ME/ARH tanycytes, of ovariectomized mice were strikingly similar to those in HFD mice, suggesting that the lack of estrogens is triggering the same molecular mechanisms as metabolic imbalances. The fact that many nNOS neurons also express the estrogen receptor ERα (*80*) could contribute to the increased risk of severe disease in men if the balance between neuroprotection and inflammation were to be altered depending on sex. Again, this is only a part of the picture, as both ACE2 and TMPRSS2 are also themselves responsive to gonadal hormones – estrogens and androgens respectively (*87, 88*).

There are no doubt several other networks that are involved both in the normal physiological and neuroendocrine functions of the hypothalamus and in viral susceptibility or pathogenicity. As an intellectual exercise, we performed enrichment for GO terms on the set of 140 genes that were both correlated with ACE2 and TMPRSS2 in the hypothalamus, and differentially expressed in the lung of COVID-19 patients. We then used the STRING database (https://string-db.org/) to build a protein-protein interaction (PPI) map using 5 GO terms for biological processes (out of 115 that were

enriched) that we felt covered the largest range of functions of interest to a potential SARS-CoV-2 infection of olfactory or neuroendocrine circuits: "regulation of secretion by cell", "vesicle-mediated transport", "immune system process", "cell surface receptor signaling pathway" and "second-messenger-mediated signaling". We obtained a PPI network (p value = 2.58e-09) that allowed us to see the functional relationships between the proteins highlighted by our analysis, including several that we were unaware of, and identify proteins that appeared to play key roles at the intersection of several functions (Fig. 7). For instance, the genes LRRK2 and SYT11 are both implicated in Parkinson Disease, an increased incidence of which was linked to the Spanish 'flu a century ago. Conversely, we noted some functional interactions that had not been taken into account, but which might be highlighted by a different choice of GO terms for enrichment. This is particularly the case with FPR2, which has previously been noted in hypothalamic microglia (*89*), and which, in addition to being able to bind viral peptides (see for example (*79, 90*)), could play a role in neurodegenerative disorders, and mediate either pro-inflammatory or anti-inflammatory mechanisms depending on the cellular and molecular pathways used (reviewed in (*91-93*)).

To summarize, our work provides proof of concept that the brain not only possesses the cellular and molecular machinery necessary to be infected, but that the hypothalamus, which harbors neural circuits regulating a number of risk factors for severe COVID-19 in addition to being linked to brainstem cardiorespiratory centers, expresses the viral receptor ACE2 and could be a preferred port of entry and target for the virus. It remains now to confirm the presence of the virus in post-mortem brains from patients suspected of having a CNS infection.

Methods

Methods, including statements of data availability and associated accession codes and references are available on line.

References

1. L. Mao *et al.*, Neurologic Manifestations of Hospitalized Patients With Coronavirus Disease 2019 in Wuhan, China. *JAMA Neurol*, (2020).
2. J. Helms *et al.*, Neurologic Features in Severe SARS-CoV-2 Infection. *N Engl J Med*, (2020).
3. N. Poyiadji *et al.*, COVID-19–associated Acute Hemorrhagic Necrotizing Encephalopathy: CT and MRI Features *Radiology*, https://doi.org/10.1148/radiol.2020201187 (2020).
4. Y. Wu *et al.*, Nervous system involvement after infection with COVID-19 and other coronaviruses. *Brain Behav Immun*, (2020).
5. P. F. Wong *et al.*, Lessons of the month 1: A case of rhombencephalitis as a rare complication of acute COVID-19 infection. *Clin Med (Lond)*, (2020).
6. Y. C. Li, W. Z. Bai, T. Hashikawa, The neuroinvasive potential of SARS-CoV2 may play a role in the respiratory failure of COVID-19 patients. *J Med Virol*, (2020).
7. G. Conde Cardona, L. D. Quintana Pajaro, I. D. Quintero Marzola, Y. Ramos Villegas, L. R. Moscote Salazar, Neurotropism of SARS-CoV 2: Mechanisms and manifestations. *J Neurol Sci* **412**, 116824 (2020).
8. F. G. De Felice, F. Tovar-Moll, J. Moll, D. P. Munoz, S. T. Ferreira, Severe Acute Respiratory Syndrome Coronavirus 2 (SARS-CoV-2) and the Central Nervous System. *Trends Neurosci*, (2020).
9. Q. Cheng, Y. Yang, J. Gao, Infectivity of human coronavirus in the brain. *EBioMedicine* **56**, 102799 (2020).

10. J. R. Lechien *et al.*, Olfactory and gustatory dysfunctions as a clinical presentation of mild-to-moderate forms of the coronavirus disease (COVID-19): a multicenter European study. *Eur Arch Otorhinolaryngol*, (2020).
11. R. Kaye, C. W. D. Chang, K. Kazahaya, J. Brereton, J. C. Denneny, 3rd, COVID-19 Anosmia Reporting Tool: Initial Findings. *Otolaryngol Head Neck Surg*, 194599820922992 (2020).
12. R. G. Wilkerson, J. D. Adler, N. G. Shah, R. Brown, Silent hypoxia: A harbinger of clinical deterioration in patients with COVID-19. *Am J Emerg Med*, (2020).
13. L. Zhou, M. Zhang, J. Wang, J. Gao, Sars-Cov-2: Underestimated damage to nervous system. *Travel Med Infect Dis*, 101642 (2020).
14. T. Moriguchi *et al.*, A first case of meningitis/encephalitis associated with SARS-Coronavirus-2. *Int J Infect Dis* **94**, 55-58 (2020).
15. A. Paniz-Mondolfi *et al.*, Central Nervous System Involvement by Severe Acute Respiratory Syndrome Coronavirus -2 (SARS-CoV-2). *J Med Virol*, (2020).
16. R. Lu *et al.*, Genomic characterisation and epidemiology of 2019 novel coronavirus: implications for virus origins and receptor binding. *Lancet* **395**, 565-574 (2020).
17. P. Zhou *et al.*, A pneumonia outbreak associated with a new coronavirus of probable bat origin. *Nature* **579**, 270-273 (2020).
18. N. Zhu *et al.*, A Novel Coronavirus from Patients with Pneumonia in China, 2019. *N Engl J Med* **382**, 727-733 (2020).
19. W. Li *et al.*, Angiotensin-converting enzyme 2 is a functional receptor for the SARS coronavirus. *Nature* **426**, 450-454 (2003).
20. C. G. K. Ziegler *et al.*, SARS-CoV-2 Receptor ACE2 Is an Interferon-Stimulated Gene in Human Airway Epithelial Cells and Is Detected in Specific Cell Subsets across Tissues. *Cell* **181**, 1016-1035 e1019 (2020).
21. M. Y. Li, L. Li, Y. Zhang, X. S. Wang, Expression of the SARS-CoV-2 cell receptor gene ACE2 in a wide variety of human tissues. *Infect Dis Poverty* **9**, 45 (2020).
22. M. F. Doobay *et al.*, Differential expression of neuronal ACE2 in transgenic mice with overexpression of the brain renin-angiotensin system. *Am J Physiol Regul Integr Comp Physiol* **292**, R373-381 (2007).
23. K. M. Elased, T. S. Cunha, F. K. Marcondes, M. Morris, Brain angiotensin-converting enzymes: role of angiotensin-converting enzyme 2 in processing angiotensin II in mice. *Exp Physiol* **93**, 665-675 (2008).
24. Y. Ding *et al.*, Organ distribution of severe acute respiratory syndrome (SARS) associated coronavirus (SARS-CoV) in SARS patients: implications for pathogenesis and virus transmission pathways. *J Pathol* **203**, 622-630 (2004).
25. J. Gu *et al.*, Multiple organ infection and the pathogenesis of SARS. *J Exp Med* **202**, 415-424 (2005).
26. J. Xu *et al.*, Detection of severe acute respiratory syndrome coronavirus in the brain: potential role of the chemokine mig in pathogenesis. *Clin Infect Dis* **41**, 1089-1096 (2005).
27. L. Wei *et al.*, Endocrine cells of the adenohypophysis in severe acute respiratory syndrome (SARS). *Biochem Cell Biol* **88**, 723-730 (2010).
28. M. K. Leow *et al.*, Hypocortisolism in survivors of severe acute respiratory syndrome (SARS). *Clin Endocrinol (Oxf)* **63**, 197-202 (2005).
29. P. Mo *et al.*, Clinical characteristics of refractory COVID-19 pneumonia in Wuhan, China. *Clin Infect Dis*, (2020).
30. W. J. Guan *et al.*, Clinical Characteristics of Coronavirus Disease 2019 in China. *N Engl J Med*, (2020).
31. C. Huang *et al.*, Clinical features of patients infected with 2019 novel coronavirus in Wuhan, China. *Lancet* **395**, 497-506 (2020).
32. Y. Yang *et al.*, Epidemiological and clinical features of the 2019 novel coronavirus outbreak in China. *medRxiv*, doi: https://doi.org/10.1101/2020.1102.1110.20021675 (2020).

33. M. Madjid, P. Safavi-Naeini, S. D. Solomon, O. Vardeny, Potential Effects of Coronaviruses on the Cardiovascular System: A Review. *JAMA Cardiol*, (2020).
34. R. E. Jordan, P. Adab, K. K. Cheng, Covid-19: risk factors for severe disease and death. *BMJ* **368**, m1198 (2020).
35. F. Zhou *et al.*, Clinical course and risk factors for mortality of adult inpatients with COVID-19 in Wuhan, China: a retrospective cohort study. *Lancet* **395**, 1054-1062 (2020).
36. J. Yang *et al.*, Prevalence of comorbidities in the novel Wuhan coronavirus (COVID-19) infection: a systematic review and meta-analysis. *Int J Infect Dis*, (2020).
37. C. Gizowski, C. W. Bourque, The neural basis of homeostatic and anticipatory thirst. *Nat Rev Nephrol* **14**, 11-25 (2018).
38. J. Clasadonte, V. Prevot, The special relationship: glia-neuron interactions in the neuroendocrine hypothalamus. *Nat Rev Endocrinol* **14**, 25-44 (2018).
39. K. S. Kim, R. J. Seeley, D. A. Sandoval, Signalling from the periphery to the brain that regulates energy homeostasis. *Nat Rev Neurosci* **19**, 185-196 (2018).
40. M. Ishii, C. Iadecola, Metabolic and Non-Cognitive Manifestations of Alzheimer's Disease: The Hypothalamus as Both Culprit and Target of Pathology. *Cell Metab* **22**, 761-776 (2015).
41. M. L. Andermann, B. B. Lowell, Toward a Wiring Diagram Understanding of Appetite Control. *Neuron* **95**, 757-778 (2017).
42. I. Fukushi, S. Yokota, Y. Okada, The role of the hypothalamus in modulation of respiration. *Respir Physiol Neurobiol* **265**, 172-179 (2019).
43. T. E. Holy, The Accessory Olfactory System: Innately Specialized or Microcosm of Mammalian Circuitry? *Annu Rev Neurosci* **41**, 501-525 (2018).
44. R. D. Palmiter, The Parabrachial Nucleus: CGRP Neurons Function as a General Alarm. *Trends Neurosci* **41**, 280-293 (2018).
45. E. H. Shen, C. C. Overly, A. R. Jones, The Allen Human Brain Atlas: comprehensive gene expression mapping of the human brain. *Trends Neurosci* **35**, 711-714 (2012).
46. D. Blanco-Melo *et al.*, Imbalanced Host Response to SARS-CoV-2 Drives Development of COVID-19. *Cell* **181**, 1036-1045 e1039 (2020).
47. I. Hamming *et al.*, Tissue distribution of ACE2 protein, the functional receptor for SARS coronavirus. A first step in understanding SARS pathogenesis. *J Pathol* **203**, 631-637 (2004).
48. C. A. Romero, M. Orias, M. R. Weir, Novel RAAS agonists and antagonists: clinical applications and controversies. *Nat Rev Endocrinol* **11**, 242-252 (2015).
49. J. Reimand *et al.*, Pathway enrichment analysis and visualization of omics data using g:Profiler, GSEA, Cytoscape and EnrichmentMap. *Nat Protoc* **14**, 482-517 (2019).
50. S. Riviere, L. Challet, D. Fluegge, M. Spehr, I. Rodriguez, Formyl peptide receptor-like proteins are a novel family of vomeronasal chemosensors. *Nature* **459**, 574-577 (2009).
51. E. Weiss, D. Kretschmer, Formyl-Peptide Receptors in Infection, Inflammation, and Cancer. *Trends Immunol* **39**, 815-829 (2018).
52. J. F. Chan *et al.*, Simulation of the clinical and pathological manifestations of Coronavirus Disease 2019 (COVID-19) in golden Syrian hamster model: implications for disease pathogenesis and transmissibility. *Clin Infect Dis*, (2020).
53. C. Garcia-Caceres *et al.*, Role of astrocytes, microglia, and tanycytes in brain control of systemic metabolism. *Nat Neurosci* **22**, 7-14 (2019).
54. F. Langlet *et al.*, Tanycytic VEGF-A Boosts Blood-Hypothalamus Barrier Plasticity and Access of Metabolic Signals to the Arcuate Nucleus in Response to Fasting. *Cell Metab* **17**, 607-617 (2013).
55. D. Wang *et al.*, Clinical Characteristics of 138 Hospitalized Patients With 2019 Novel Coronavirus-Infected Pneumonia in Wuhan, China. *JAMA*, (2020).
56. F. A. Klok *et al.*, Incidence of thrombotic complications in critically ill ICU patients with COVID-19. *Thromb Res*, (2020).
57. J. Helms *et al.*, High risk of thrombosis in patients with severe SARS-CoV-2 infection: a multicenter prospective cohort study. *Intensive Care Med*, (2020).

58. M. M. Lamers *et al.*, SARS-CoV-2 productively infects human gut enterocytes. *Science*, (2020).
59. Z. Li *et al.*, Neurological manifestations of patients with COVID-19: potential routes of SARS-CoV-2 neuroinvasion from the periphery to the brain. *Front Med*, (2020).
60. S. Natoli, V. Oliveira, P. Calabresi, L. F. Maia, A. Pisani, Does SARS-Cov-2 invade the brain? Translational lessons from animal models. *Eur J Neurol*, (2020).
61. W. G. Glass, K. Subbarao, B. Murphy, P. M. Murphy, Mechanisms of host defense following severe acute respiratory syndrome-coronavirus (SARS-CoV) pulmonary infection of mice. *J Immunol* **173**, 4030-4039 (2004).
62. P. B. McCray, Jr. *et al.*, Lethal infection of K18-hACE2 mice infected with severe acute respiratory syndrome coronavirus. *J Virol* **81**, 813-821 (2007).
63. J. Netland, D. K. Meyerholz, S. Moore, M. Cassell, S. Perlman, Severe acute respiratory syndrome coronavirus infection causes neuronal death in the absence of encephalitis in mice transgenic for human ACE2. *J Virol* **82**, 7264-7275 (2008).
64. C. T. Tseng *et al.*, Severe acute respiratory syndrome coronavirus infection of mice transgenic for the human Angiotensin-converting enzyme 2 virus receptor. *J Virol* **81**, 1162-1173 (2007).
65. L. S. Politi, E. Salsano, M. Grimaldi, Magnetic Resonance Imaging Alteration of the Brain in a Patient With Coronavirus Disease 2019 (COVID-19) and Anosmia. *JAMA Neurol*, (2020).
66. K. Bilinska, P. Jakubowska, C. S. Von Bartheld, R. Butowt, Expression of the SARS-CoV-2 Entry Proteins, ACE2 and TMPRSS2, in Cells of the Olfactory Epithelium: Identification of Cell Types and Trends with Age. *ACS Chem Neurosci*, (2020).
67. E. Milanetti *et al.*, In-Silico evidence for two receptors based strategy of SARS-CoV-2. *arXiv*, arXiv:2003.11107 (2020).
68. C. J. Sigrist, A. Bridge, P. Le Mercier, A potential role for integrins in host cell entry by SARS-CoV-2. *Antiviral Res* **177**, 104759 (2020).
69. F. Casoni *et al.*, Development of the neurons controlling fertility in humans: new insights from 3D imaging and transparent fetal brains. *Development* **143**, 3969-3981 (2016).
70. J. A. Jaimes, N. M. Andre, J. S. Chappie, J. K. Millet, G. R. Whittaker, Phylogenetic Analysis and Structural Modeling of SARS-CoV-2 Spike Protein Reveals an Evolutionary Distinct and Proteolytically Sensitive Activation Loop. *J Mol Biol*, (2020).
71. S. Bertram *et al.*, Cleavage and activation of the severe acute respiratory syndrome coronavirus spike protein by human airway trypsin-like protease. *J Virol* **85**, 13363-13372 (2011).
72. W. Chen *et al.*, Detectable 2019-nCoV viral RNA in blood is a strong indicator for the further clinical severity. *Emerg Microbes Infect* **9**, 469-473 (2020).
73. A. Mullier, S. G. Bouret, V. Prevot, B. Dehouck, Differential distribution of tight junction proteins suggests a role for tanycytes in blood-hypothalamus barrier regulation in the adult mouse brain. *J Comp Neurol* **518**, 943-962 (2010).
74. F. Langlet, A. Mullier, S. G. Bouret, V. Prevot, B. Dehouck, Tanycyte-like cells form a blood-cerebrospinal fluid barrier in the circumventricular organs of the mouse brain. *J Comp Neurol* **521**, 3389-3405 (2013).
75. I. Ferrer *et al.*, Olfactory Receptors in Non-Chemosensory Organs: The Nervous System in Health and Disease. *Front Aging Neurosci* **8**, 163 (2016).
76. N. N. Patel, A. D. Workman, N. A. Cohen, Role of Taste Receptors as Sentinels of Innate Immunity in the Upper Airway. *J Pathog* **2018**, 9541987 (2018).
77. A. Salas *et al.*, Whole Exome Sequencing reveals new candidate genes in host genomic susceptibility to Respiratory Syncytial Virus Disease. *Sci Rep* **7**, 15888 (2017).
78. S. Tcherniuk *et al.*, Formyl Peptide Receptor 2 Plays a Deleterious Role During Influenza A Virus Infections. *J Infect Dis* **214**, 237-247 (2016).
79. P. B. Ampomah, L. A. Moraes, H. M. Lukman, L. H. K. Lim, Formyl peptide receptor 2 is regulated by RNA mimics and viruses through an IFN-beta-STAT3-dependent pathway. *FASEB J* **32**, 1468-1478 (2018).

80. K. Chachlaki *et al.*, Phenotyping of nNOS neurons in the postnatal and adult female mouse hypothalamus. *J Comp Neurol* **525**, 3177-3189 (2017).
81. K. Chachlaki, J. Garthwaite, V. Prevot, The gentle art of saying NO: how nitric oxide gets things done in the hypothalamus. *Nat Rev Endocrinol* **13**, 521-535 (2017).
82. K. Chachlaki, V. Prevot, Nitric oxide signalling in the brain and its control of bodily functions. *Br J Pharmacol*, doi: 10.1111/bph.14800. (2019).
83. A. Jais, J. C. Bruning, Hypothalamic inflammation in obesity and metabolic disease. *J Clin Invest* **127**, 24-32 (2017).
84. S. Akerstrom *et al.*, Nitric oxide inhibits the replication cycle of severe acute respiratory syndrome coronavirus. *J Virol* **79**, 1966-1969 (2005).
85. X. Chen *et al.*, Fpr2 Deficiency Alleviates Diet-Induced Insulin Resistance Through Reducing Body Weight Gain and Inhibiting Inflammation Mediated by Macrophage Chemotaxis and M1 Polarization. *Diabetes* **68**, 1130-1142 (2019).
86. M. Bottcher *et al.*, NF-kappaB signaling in tanycytes mediates inflammation-induced anorexia. *Mol Metab*, 101022 (2020).
87. K. E. Stelzig *et al.*, Estrogen regulates the expression of SARS-CoV-2 receptor ACE2 in differentiated airway epithelial cells. *Am J Physiol Lung Cell Mol Physiol*, (2020).
88. B. Lin *et al.*, Prostate-localized and androgen-regulated expression of the membrane-bound serine protease TMPRSS2. *Cancer Res* **59**, 4180-4184 (1999).
89. H. Wang *et al.*, Increased hypothalamic microglial activation after viral-induced pneumococcal lung infection is associated with excess serum amyloid A production. *J Neuroinflammation* **15**, 200 (2018).
90. S. Schloer *et al.*, The annexin A1/FPR2 signaling axis expands alveolar macrophages, limits viral replication, and attenuates pathogenesis in the murine influenza A virus infection model. *FASEB J* **33**, 12188-12199 (2019).

Acknowledgments: The authors are grateful to Dr. Nihal Altan-Bonnet for her valuable insights on the biology of SARS-CoV-2. They would also like to thank Meryem Tardivel (Confocal microscopy) and Nathalie Jouy (FACS) from the BioImaging Center of Lille (BiCeL), and Julien Devassine (animal core facility) of the UMS2014-US41 for their expert technical support. **Funding**. This work was supported by the European Research Council (ERC) Synergy Grant-2019-WATCH-810331 to V. P, EGID to V.P. and DistAlz (to V.P. F.P.). **Author contributions**: S.R. and V.P. designed the study, analyzed data, prepared the figures, and wrote the manuscript. S.N. designed and performed the bioinformatics analyses, and was involved in all aspects of study design, interpretation of results, and manuscript preparation; F.S., G.T., D.F., C.C., M.I. and E.D. prepared tissues and performed the immunofluorescence and RTqPCR analyses; R.P., V.F., M.B., F.P., F.T., C.A.-M, V.M. and P.G. were involved in the study design, interpretation of the results, and preparation of the manuscript. **Competing interests**: The authors declare no competing interests. Data and materials availability: all data are available in the main text or the supplementary materials.

Supplementary Materials:

Materials and Methods
Figures S1-S10
References (*91-99*)

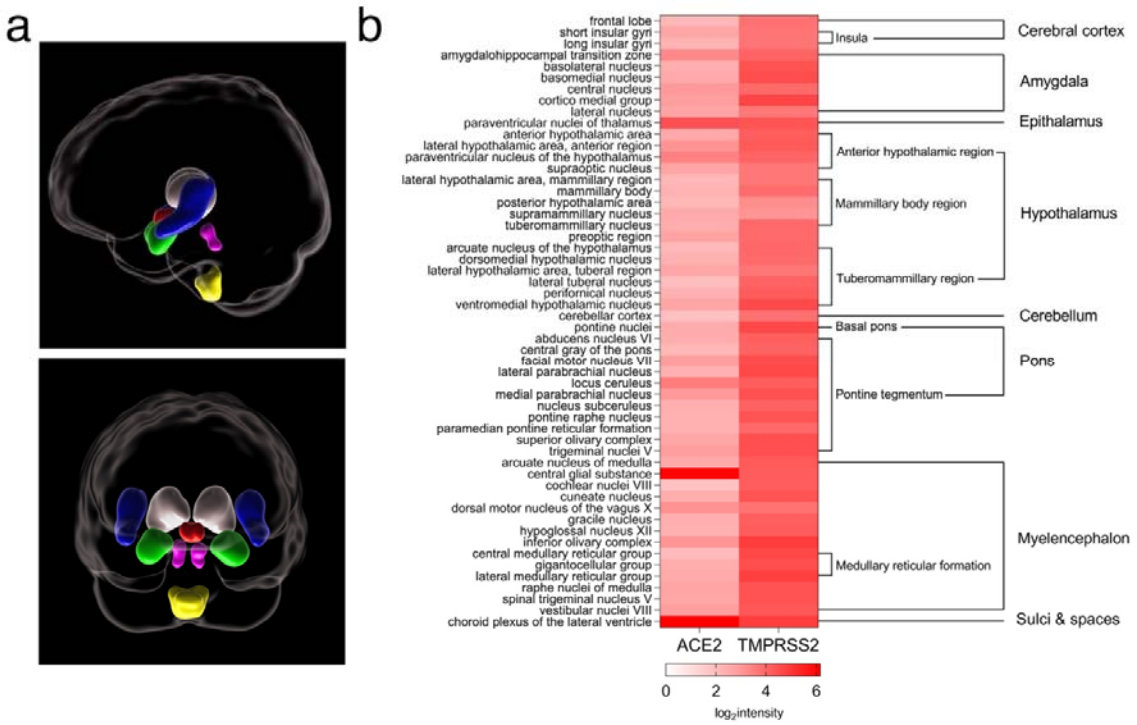

Figure 1. ACE2 and TMPRSS2 are expressed in the human hypothalamus and connected brain regions. (**a**) Schematic of brain regions analyzed in the AHBA in sagittal (top) and frontal (bottom) views. Insula: blue, amygdala: green, thalamus: grey, hypothalamus: red, pons (parabrachial nucleus): pink, myelencephalon: yellow. The frontal lobe of the cerebral cortex, the cerebellar cortex and the choroid plexus were analyzed for comparison but not shown here. (**b**) Heat Map of ACE2 and TMPRSS2 showing log2 expression values in various nuclei or subregions (left) in the different brain regions studied (right).

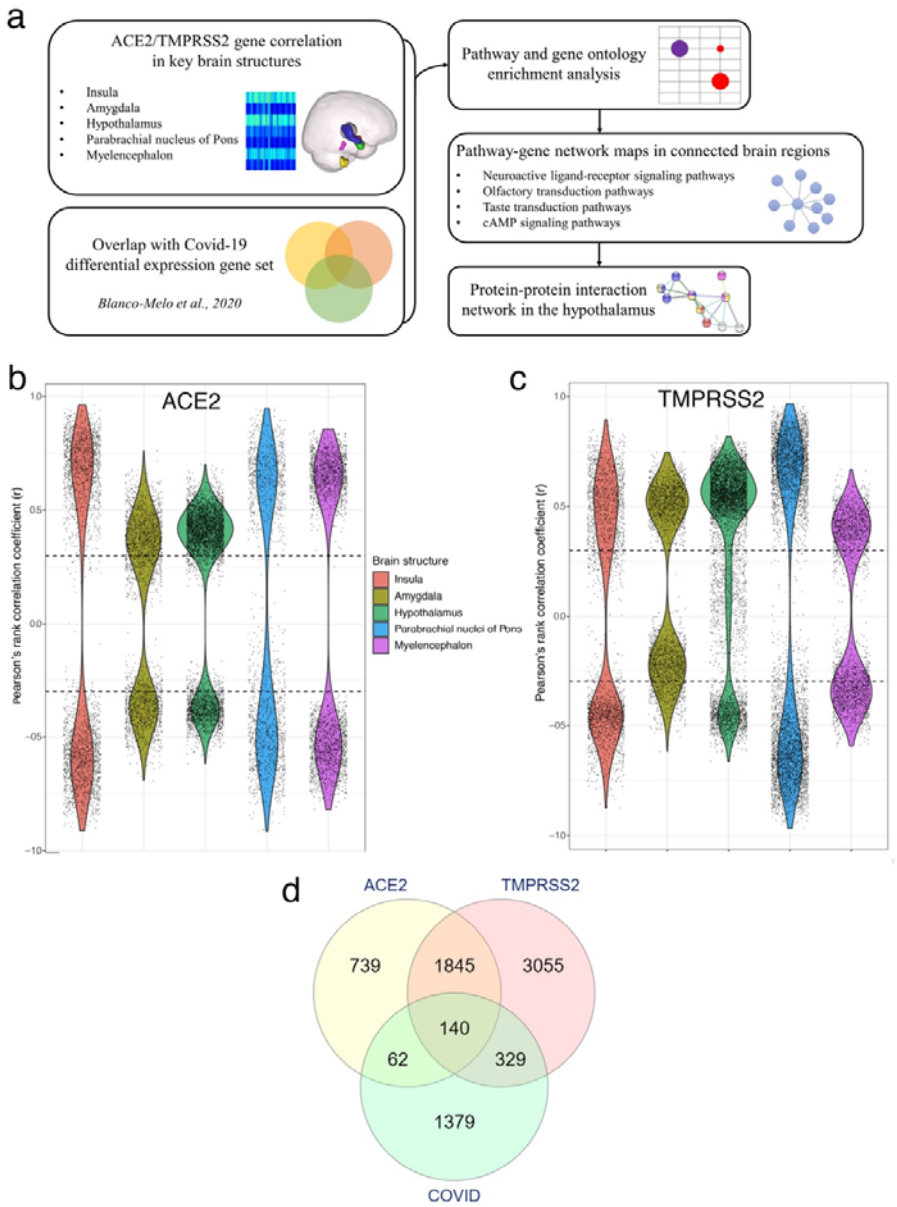

Figure 2. Genes correlated with ACE2/TMPRSS2 and SARS-CoV-2 lung infection in key brain regions. (**a**) Schematic of correlation and interaction analyses of gene-expression data from the AHBA. (**b**,**c**) Violin plots showing number and distribution by Pearson's rank correlation coefficient (r) of ACE2- and TMPRSS- correlated genes in 5 brain regions. (**d**) Venn diagram showing overlap of hypothalamic ACE2- and/orTMPRSS2-correlated genes (-0.3 < r < 0.3; fdr < 0.25) with COVID-19 patient lung geneset (*46*).

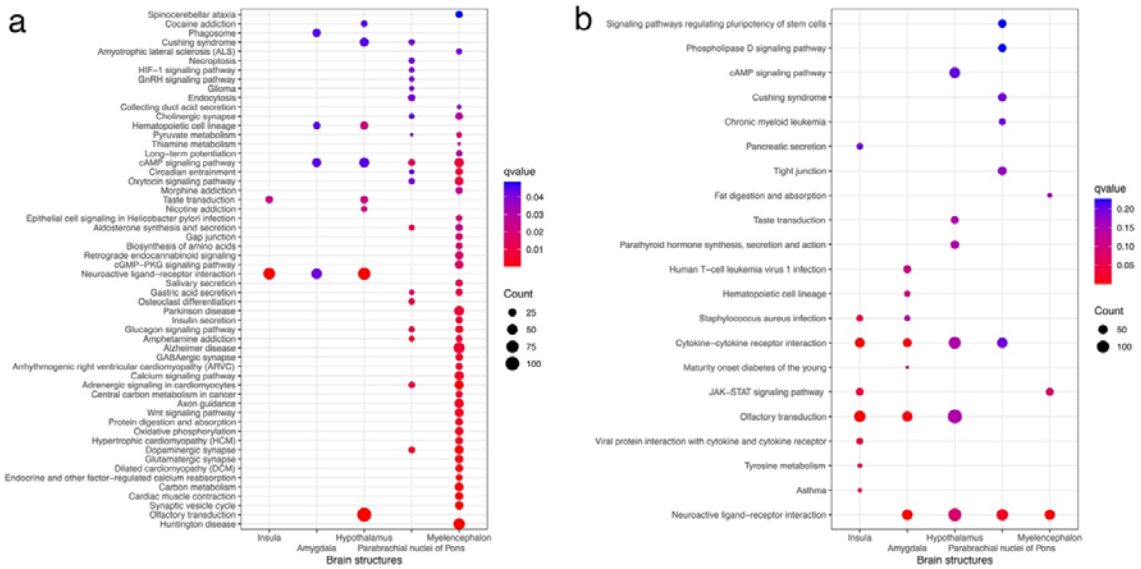

Figure 3. ACE2/TMPRSS2-correlated genes are involved in functional networks of interest. (**a**,**b**) Most significant KEGG pathways yielded by gene enrichment for ACE2-correlated (**a**) and TMPRSS2-correlated genes (**b**) in each of the 5 regions of interest. q value cutoff was set at 0.05 for ACE2 in this figure due to the very large number of significant pathways. Otherwise, q value cutoff was set at an acceptable exploratory level of 0.25. Note that the pathways with the highest number of enriched genes (Count) are in the hypothalamus for both genes queried.

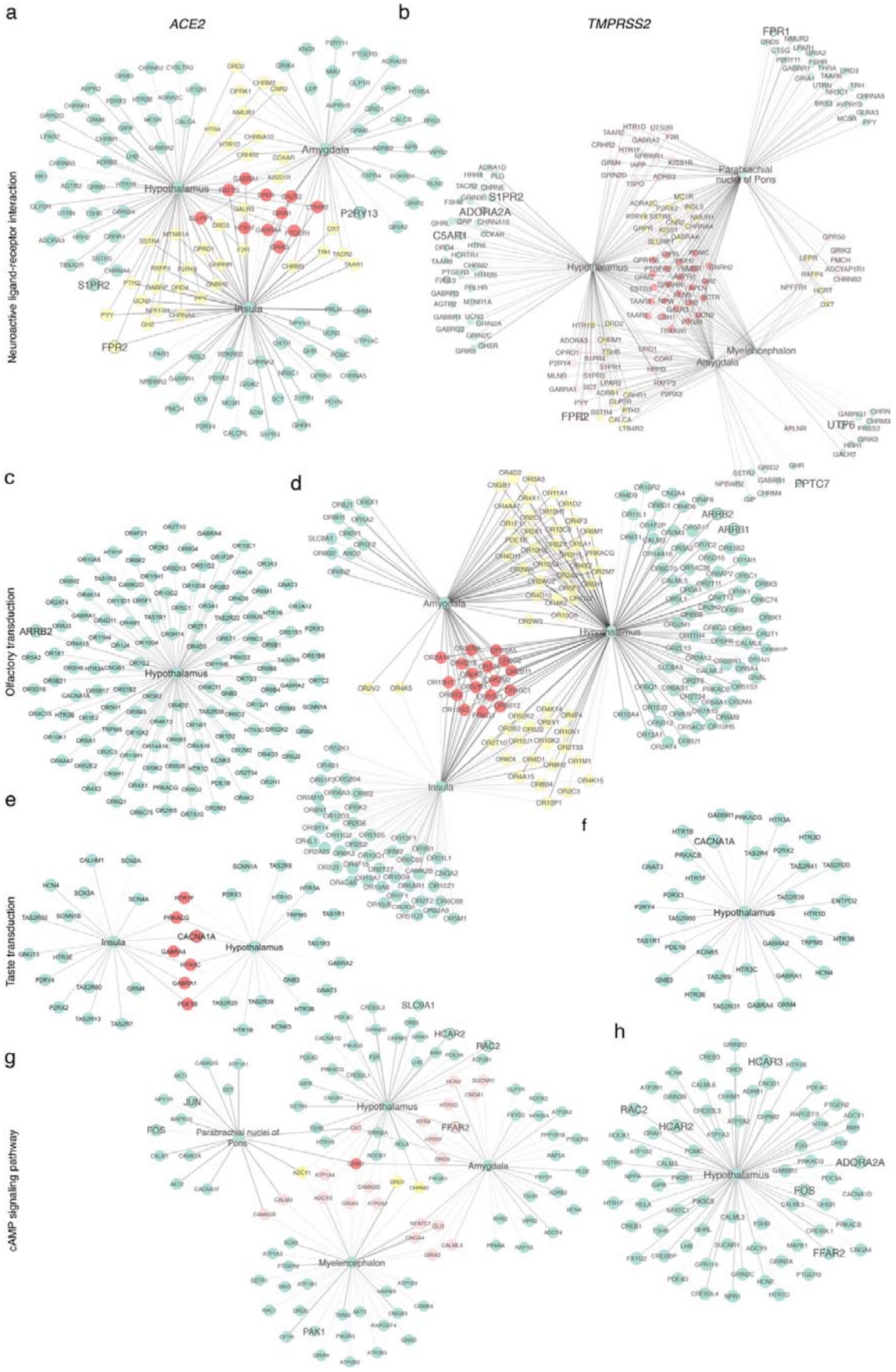
a
ACE2
Neuroactive ligand-receptor interaction
Amygdala
Hypothalamus
P2RY13
S1PR2
FPR2
Insula
b
TMPRSS2
FPR1
Parabrachial nuclei of Pons
S1PR2
ADORA2A
C5AR1
Hypothalamus
Myelencephalon
Amygdala
FPR2
UTP6
c
Olfactory transduction
ARRB2
Hypothalamus
d
Amygdala
Hypothalamus
Insula
ARRB2
ARRB1
PPTC7
e
Taste transduction
Insula
CACNA1A
Hypothalamus
f
CACNA1A
Hypothalamus
g
cAMP signaling pathway
JUN
FOS
Parabrachial nuclei of Pons
Hypothalamus
FFAR2
Amygdala
Myelencephalon
PAK1
SLC9A1
HCAR2
RAC2
h
HCAR3
RAC2
HCAR2
Hypothalamus
ADORA2A
FOS
FFAR2

Figure 4. Functionally connected brain regions express common ACE2- and TMPRSS2-correlated genes and pathways. Network of ACE2- and TMPRSS2-correlated genes showing common genes in the four most ubiquitous KEGG pathways in all brain regions where they are enriched. (**a**,**b**) KEGG pathway network for "neuroactive ligand-receptor interaction". (**c**,**d**) KEGG pathway network for "olfactory transduction". (**e**,**f**) KEGG pathway network for "taste transduction". (**g**,**h**) KEGG pathway network for "cAMP signaling pathway". Node colors: red = genes common to all the regions in which enriched (**a,b,d,e,g**); yellow = genes common to 2 (**a,d**) or 3 (**b,g**) regions in which enriched; pink = genes common to 2 regions in which enriched (**b,g**); green = genes found in only one region. Genes also common to the COVID-19 patient lung dataset are indicated in larger font in all networks.

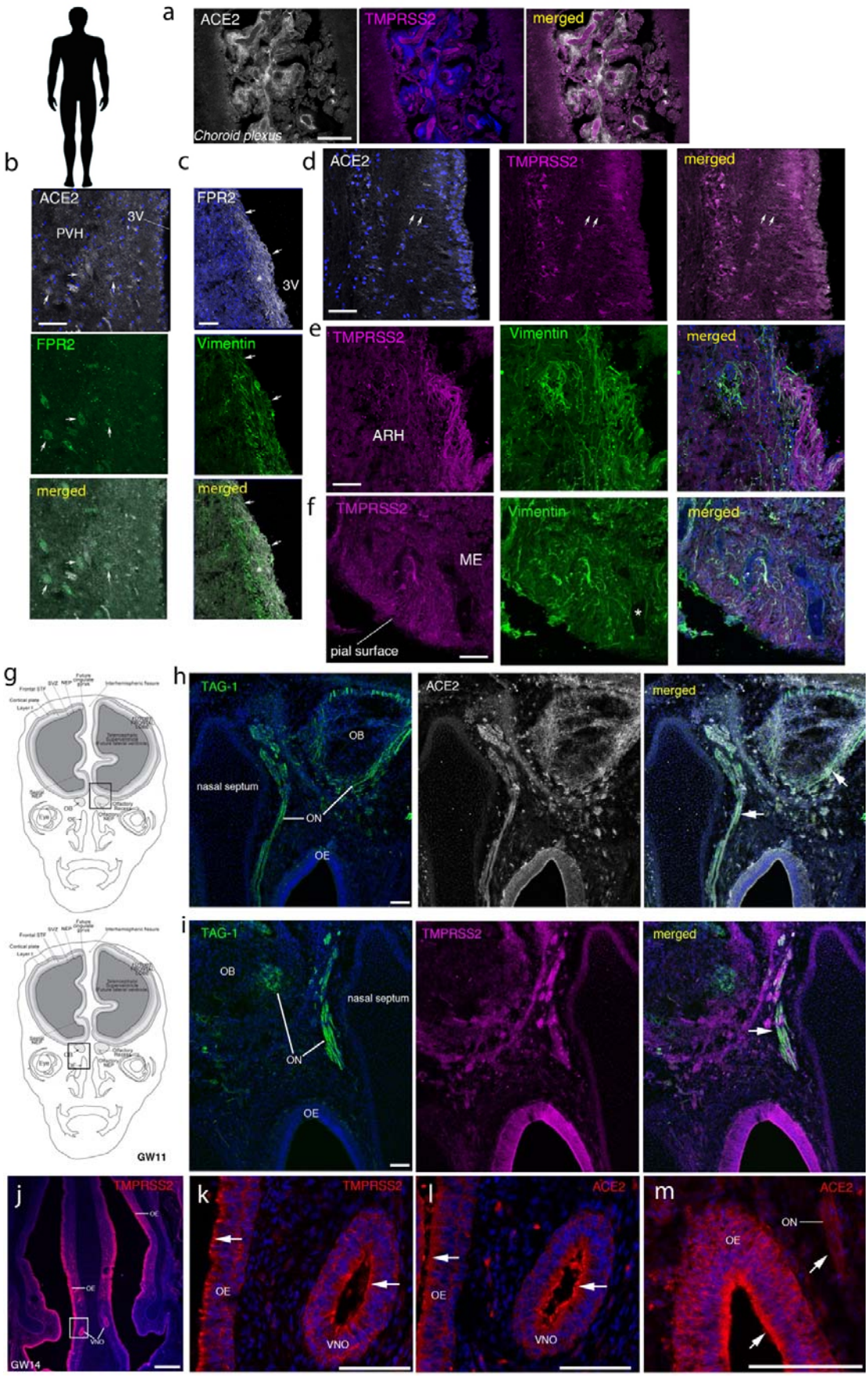
a
ACE2
TMPRSS2
merged
Choroid plexus
b
ACE2
3V
PVH
FPR2
merged
c
FPR2
3V
Vimentin
merged
d
ACE2
TMPRSS2
merged
e
TMPRSS2
ARH
Vimentin
merged
f
TMPRSS2
ME
pial surface
Vimentin
merged
g
GW11
h
TAG-1
OB
nasal septum
ON
OE
ACE2
merged
i
TAG-1
OB
nasal septum
ON
OE
TMPRSS2
merged
j
TMPRSS2
OE
VNO
GW14
k
TMPRSS2
OE
VNO
l
ACE2
OE
VNO
m
ACE2
ON
OE

Figure 5. Immunolabeling for ACE2 and TMPRSS2 in the adult human brain and embryonic human nose and olfactory bulb. (**a**) In control adult human brains, ACE2 (white; anti-human ACE2 antibody) and TMPRSS2 (magenta) are present abundantly in the choroid plexus. (**b**) ACE2 is also more sparsely present in neurons of the PVH (solid arrows), where it colocalizes with FPR2 (green). (**c**) Closer to the ventricular wall, FPR2 labeling (white) occurs in fibers of unknown origin but does not colocalize with the tanycytic marker vimentin (green). (**d**) ACE2 (white) is also present at low levels and colocalized with TMPRSS2 (magenta) in tanycytic processes bordering the 3V (arrows). (**e,f**) TMPRSS2 (magenta) is strongly expressed in vimentin-positive (green) tanycytes in the ARH and ME. (**g**) Schematic diagram of the cross section of an embryonic head at gestational week (GW) 11, showing areas represented. Boxes in (**g**) depict the areas shown in the photomicrographs in (**h,i**). (**h,i**) ACE2 (**h**, white) and TMPRSS2 (**i**, magenta) colocalize (white arrows) with TAG-1 (green), a marker of the axon tracts in the primary olfactory region (olfactory nerve, ON) and of vomeronasal axons, which, at this stage, start projecting to the presumptive olfactory bulbs (OB). (**j,k,l,m**) Olfactory and vomeronasal sensory neurons, along with other supporting cells, strongly express ACE2 (**l,m**) or TMPRSS2 (**k**) (both red, white arrows). Blue: DAPI. VNO: presumptive vomeronasal organ. STF: stratified transitional fields; SVZ, subventricular zone; NEP: neuroepithelium. All scale bars = 100 µm.

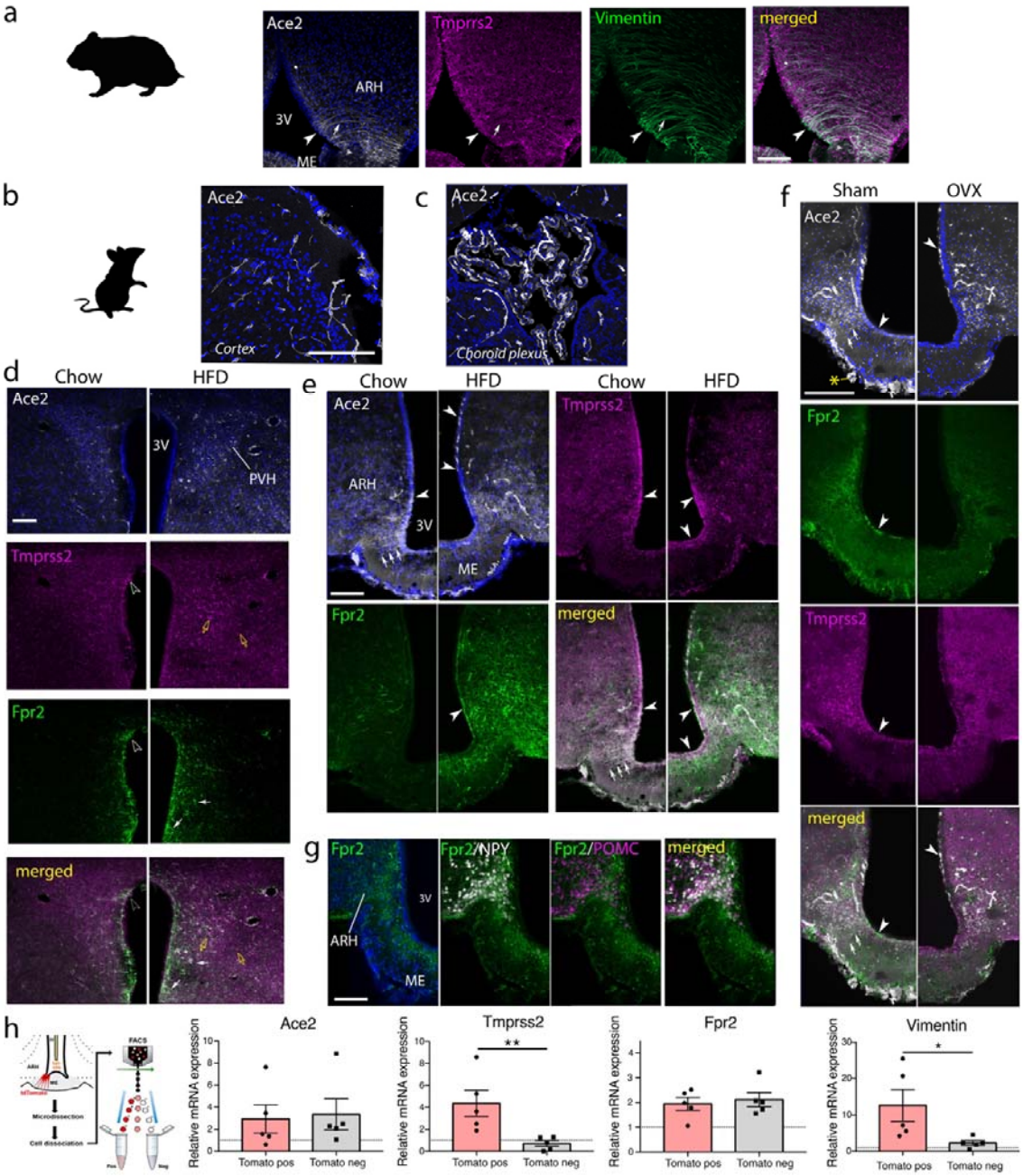

Figure 6. Immunolabeling for ACE2, TMPRSS2 and FPR2 is present and upregulated by high-fat diet in the hypothalamus of mice and hamsters. (**a**) In the ARH and ME of hamsters, ACE2 (white; anti-human ACE2 antibody) and TMPRSS2 (magenta) are colocalized with the tanycytic marker vimentin (green) in both cell bodies bordering the 3V (solid arrowhead) and in processes (solid arrow). (**b,c**) Control regions. In the mouse cerebral cortex, ACE2 (white; anti mouse ACE2 antibody) is limited to the vascular walls (**b**), but it is highly expressed in a polarized pattern in cells of the choroid plexus of the lateral ventricle (**c**). (**d**) ACE2, TMPRSS2 and FPR2 immunolabeling in the paraventricular nucleus of the hypothalamus (PVH), in male mice fed a standard chow diet (left) or a high-fat diet (HFD; right). ACE2 (white) appears to be present in scattered neurons and vascular cells in chow-fed animals, and increases in HFD animals. TMPRSS2 (magenta) is expressed in a few cells with astrocytic

morphology at the ventricular wall (empty arrowhead) and scattered microglia-like cells (yellow arrows), with increased expression in the latter in HFD animals. FPR2 (green) is strongly expressed in cells with an astrocytic morphology at the ventricular wall, including in some TMPRSS2-positive cells. It is also present in astrocyte-like cells in the parenchyma near the ventricle. HFD strongly increases the number and area occupied by FPR2-positive cells. 3V: third ventricle. (**e**) ACE2 expression (white) in the hypothalamic arcuate nucleus (ARH) and median eminence (ME) occurs in ME tanycytic cell bodies and processes as well as some blood vessels, and in the highly vascularized pars tuberalis under the ME. In HFD animals, ACE2 expression in ME tanycytic cell bodies is reduced and processes are no longer labeled, but labeling appears at the apical pole of tanycytes further up the ventricular wall and increases greatly in capillary walls in the ARH. The labeling in the pars tuberalis is also reduced. TMPRSS2, also present in tanycytic cell bodies and processes, increases slightly with HFD. FPR2, which appears to be in microglia-like cells in the ME and ARH and the cell bodies of tanycytes, increases strongly. (**f**) ACE2 (white), TMPRSS2 (magenta) and FPR2 (green) immunolabeling in the ARH and ME of ovariectomized (OVX) female mice showing changes in ACE2 and TMPRSS2 similar to that seen in male HFD mice. FPR2 labeling, however, appears to be less intense and in different cell types or components from that in males. (**g**) FPR2 immunolabeling (green) in tanycytic processes and microglia-like cells in the ARH and EM of transgenic mice expressing NPY-GFP (white) and POMC:Cre; tdTomato mice (magenta). Blue: DAPI. Scale bars = 100 µm. (**h**) FACS-based sorting of tdTomato-positive (pos) and negative (neg) cells from the mediobasal hypothalamus of mice expressing tdTomato exclusively in tanycytes (top panel) to confirm cell-type-specific labeling seen in (**e,f**) for ACE2, TMPRSS2 and FPR2. Vimentin (bottom panel) was used to confirm the purity of FACSed cells. *$p<0.05$, **$p<0.01$, Mann-Whitney test.

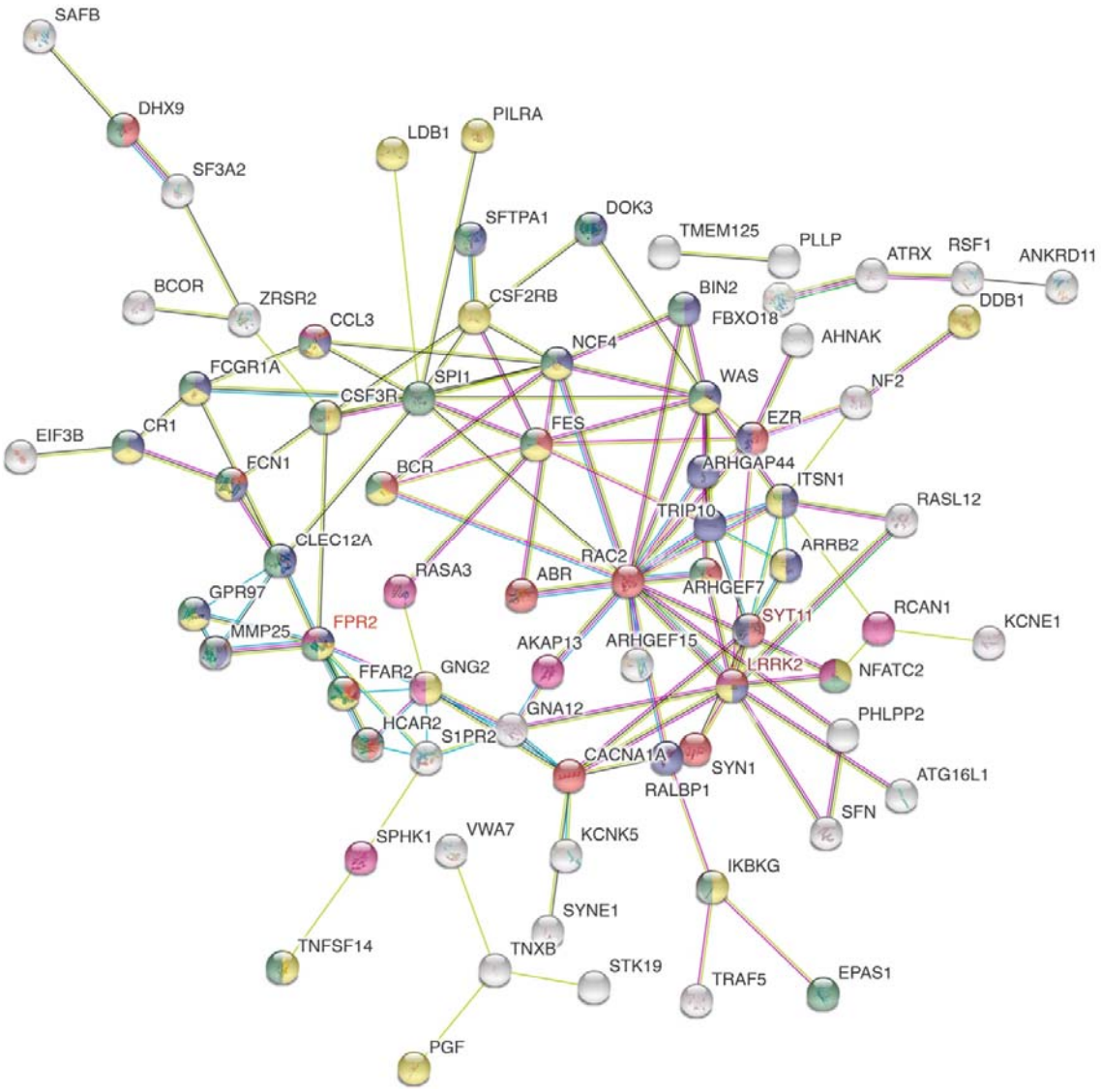

Figure 7. Sample protein-protein interaction map of GO terms of importance to hypothalamic function and viral pathogenesis. Common genes between ACE2-/TMPRSS2-correlated genes in the hypothalamus and the COVID-19 lung differentially expressed geneset were enriched for GO terms for biological processes and queried with STRING to obtain functional protein-protein interaction (PPI) networks using 5 diverse terms of interest: "regulation of secretion by cell" (red), "vesicle-mediated transport" (blue), "immune system process" (green), "cell surface receptor signaling pathway" (yellow), "second-messenger-mediated signaling" (violet). White proteins are connectors not themselves present in our genesets. Empty nodes are those whose structure is not known. Proteins with no interactions highlighted by our analysis were removed to simplify the figure. Note that FPR2 is among the 4 proteins that appear under the most GO terms selected (4 out of 5), along with CCL3, FCN1 and LRRK2. Edge color code for associations: turquoise – known interactions from curated databases; magenta – experimentally determined known interactions; green – predicted interaction based on gene neighborhood; red – predicted interaction based on gene fusions; dark blue – predicted interactions based on gene co-occurrence; yellow – textmining; black –

coexpression; pale blue – protein homology. Edges indicate that proteins jointly contribute to a shared function, without necessarily binding to each other.

Table 1. Enriched genes common to multiple regions and the COVID-19 lung dataset. The gene sets identified by our enrichment for the 4 KEGG pathways of interest were cross-checked against the geneset obtained from the COVID-19 lung (*46*), and the common genes annotated below.

Gene symbol	Gene name	log2 FoldChange COVID vs. healthy lung (*46*)	Pathways	Correlation in Brain structure	Gene with which correlated	r value
FPR2	N-formyl peptide receptor 2	+2.476	Neuroactive ligand-receptor Interaction	Insula Hypothalamus	ACE2	+0.493 +0.695
			Neuroactive ligand-receptor Interaction	Hypothalamus Amygdala	TMPRSS2	+0.637 +0.376
FPR1	Formyl Peptide Receptor 1	+3.933	Neuroactive ligand-receptor Interaction	Parabrachial Nucleus	TMPRSS2	+0.645
P2RY13	P2Y purinoceptor 13	+6.473	Neuroactive ligand-receptor Interaction	Amygdala	ACE2	+0.515
S1PR2	Sphingosine-1-phosphate receptor	-3.566	Neuroactive ligand-receptor Interaction	Hypothalamus	ACE2	+0.331
				Hypothalamus	TMPRSS2	+0.512
UTP6	UTP6 Small Subunit Processome Component	-3.078	Neuroactive ligand-receptor Interaction	Myelencephalon	TMPRSS2	-0.499
C5AR1	Complement C5a Receptor 1	+2.473	Neuroactive ligand-receptor Interaction	Hypothalamus	TMPRSS2	+0.533
ADORA 2A	Adenosine A2a Receptor	-3.207	Neuroactive ligand-receptor Interaction	Hypothalamus	TMPRSS2	+0.479
			cAMP signaling			
PPTC7	Protein Phosphatase Targeting COQ7	-3.158	Neuroactive ligand-receptor Interaction	Amygdala	TMPRSS2	-0.416
ARRB2	Arrestin Beta 2	+3.620	Olfactory transduction	Hypothalamus	ACE2	+0.489
					TMPRSS2	+0.5998
ARRB1	Arrestin Beta 1	-2.511	Olfactory transduction	Hypothalamus	TMPRSS2	+0.463
CACNA 1A	Calcium Voltage-Gated Channel Subunit Alpha1 A	+4.767	Taste transduction	Hypothalamus Insula	ACE2	+0.487 +0.663
				Hypothalamus	TMPRSS2	+0.578
SLC9A1	Solute Carrier	-3.733	cAMP signaling	Hypothalamus	ACE2	-0.356

	Family 9 Member A1					
JUN	Jun Proto-Oncogene, AP-1 Transcription Factor Subunit	-3.572	cAMP signaling	Parabrachial nuclei of Pons	ACE2	-0.794
ATP1A1	ATPase Na+/K+ Transporting Subunit Alpha 1	-2.043	cAMP signaling	Parabrachial nuclei of Pons	ACE2	+0.854
PAK1	P21 (RAC1) Activated Kinase 1	+2.042	cAMP signaling	Myelencephalon	ACE2	-0.559
HCAR2	Hydroxycarboxylic Acid Receptor 2	+2.777	cAMP signaling	Hypothalamus	ACE2	+0.586
					TMPRSS2	+0.599
FOS	Fos Proto-Oncogene, AP-1 Transcription Factor Subunit	-5.309	cAMP signaling	Parabrachial nuclei of Pons	ACE2	-0.715
				Hypothalamus	TMPRSS2	-0.494
FFAR2	Free Fatty Acid Receptor 2	+6.696	cAMP signaling	Amygdala Hypothalamus	ACE2	+0.451 +0.534
				Hypothalamus	TMPRSS2	+0.541
RAC2	Ras-related C3 botulinum toxin substrate 2	+3.546	cAMP signaling	Hypothalamus	ACE2	+0.431
			cAMP signaling	Hypothalamus	TMPRSS2	+0.640
RAPGEF 3	Rap Guanine Nucleotide Exchange Factor 3	-3.793	cAMP signaling	Hypothalamus	TMPRSS2	+0.560

Supplementary Materials

Materials and Methods

Gene expression analysis for ACE2, TMPRSS2 and correlated genes in the brain

Differential distribution of ACE2 and TMPRSS2 across brain regions

Normalized gene expression values of ACE2 and TMPRSS2 were retrieved from the Allen Human Brain Atlas (AHBA) (*45*) for nuclei of the hypothalamus, insula, amygdala, paraventricular nucleus of the thalamus, pons and myelencephalon. The frontal lobe and cerebellar cortex as well as the choroid plexus were included for comparison. The probes were mapped to ACE2 and TMPRSS2 genes using the *collapseRows* function of WGCNA_1.69-81 (*94*) in R ver3.6.3. Probe *CUST_16267_PI416261804* for ACE2 and probe *A_23_P29067* for TMPRSS2 were selected based on maximum variance across all samples (maxRowVariance of WGCNA package). The data were concatenated across all donors for the specified brain structures. To account for missing ACE2 and TMPRSS2 expression values for the brain structures excluded for various technical reasons such as damaged or missing tissue or low-quality RNA (Allen Human Brain Atlas, technical white paper: microarray survey), nonparametric missing value imputation was performed using R-package missForest (*95*). Median expression values of ACE2 and TMPRSS2 across all donors were presented in the form of a heatmap using GraphPad Prism 8.

ACE2/TMPRSS2-correlated genes in key brain structures

For the selected ACE2 and TMPRSS2 probes, the "positive" and "anti-correlated" genes with their normalized log2intensity gene expression values were retrieved using *"Find Correlates" search utility in* the AHBA (with a cut-off of -0.3 > r > 0.3 as in the AHBA, where r is Pearson's rank correlation coefficient) for the brain structures of interest – insula, amygdala, hypothalamus, parabrachial nuclei of pons and myelencephalon - sampled in all human donors. After filtering the probes with zero entrez-id, the expression values of the retrieved gene list were used as vector elements to recompute Pearson's correlation coefficients (r) of all gene pairs using the rcorr function of R-package Hmisc (https://cran.r-project.org/web/packages/Hmisc/index.html). The rcorr function returns a correlation matrix with the r values and the corresponding asymptotic p value based on t distribution. The function p.adjust and the method 'fdr' were applied to control for false discovery rate (fdr). ACE2- and TMPRSS2-correlated genes were extracted from the correlation matrix and filtered by (i) setting a threshold of -0.3 > r > 0.3 and fdr < 0.25, and (ii) selecting the correlations with the lowest fdr value for probes mapped to multiple genes.

COVID-19 lung RNA sequencing dataset

Raw read counts from COVID-19 infected and uninfected human lung (n=2) RNA-seq dataset were collected from GSE147507 (*46*) followed by differential expression analysis using DESeq2 (*96*). The differentially expressed genes were checked for the overlapping gene count between the COVID-19 dataset and the ACE2- and TMPRSS2-correlated gene sets.

KEGG pathway and gene ontology enrichment analyses

KEGG pathway and gene ontology (GO) enrichment analyses of ACE2- and TMPRSS2-correlated genes was performed using *Clusterprofiler* package in R (*97*), a widely used R package for enrichment analyses. enrichGO and enrichKEGG functions based on hypergeometric distributions were applied to perform the enrichment test for the ACE2 and TMPRSS2 correlated gene sets. q value cut-off (for fdr) was consistently maintained at 0.25. The enriched pathways for ACE2 and TMPRSS2 correlated genes for the analyzed brain structures were compiled together and visualized using the ggplot2 package of R. The enriched pathway-gene networks were generated using the cnetplot function of the *Clusterprofiler* package.

Gene-network maps connecting brain regions

The gene network maps connecting brain regions with shared pathways such as neuroactive ligand receptor interaction, olfactory transduction, taste transduction and cAMP signaling enriched for ACE2- and TMPRSS2-correlated genes were generated by curating genes associated with each pathway and projecting them in the form of networks using Cytoscape v3.8.0. Furthermore, these genes were checked for overlap with the COVID-19 differential gene expression dataset.

Functional protein-protein interaction network in the hypothalamus

Common genes between the COVID-19 differentially expressed geneset and ACE2-/TMPRSS2-correlated genes in the hypothalamus, were queried in the STRING database to obtain functional protein-protein (PPI) interaction networks, and the associated GO terms enriched for biological processes.

Immunofluorescence labeling – Animal brains

Animals

Mice: Three C57BL/6J (Charles River) and two NPY::GFP (JAX:006417); POMC::Cre (JAX:005965); tdTomato (JAX:007914) male mice, 8–9 weeks-old were individually housed and given ad libitum access to water and standard pelleted rodent chow (R03-25, Safe diet). Three other C57BL/6J were given ad libitum water and a high-fat diet containing 60% fat (HFD; D12492 Research Diet) for 9 weeks. Ovariectomy (OVX) in mice: 6 adult female mice against a background of C57BL/6J (ERa flox with VH injection) were subjected to ovarietomy (OVX; N=3) or sham (N=3) surgery. Briefly, OVX was performed under isoflurane anesthesia. A mid-ventral incision was made, the muscle separated gently by forceps to expose ovaries and periovarian fat tissue. Ovaries and ovarian fat were removed bilaterally after ligation of the most proximal portion of the oviduct. In sham animals, the same procedure was carried out except for the removal of the ovaries. The surgical incision was sutured and postsurgical recuperation was monitored daily. Animals were kept for 6 weeks after surgery.
Hamsters: Two 8-week (100 g) male hamsters (Janvier) were fed ad libitum and single-housed. Animal studies were performed with the approval of the Institutional Ethics Committees for the Care and Use of Experimental Animals of the University of Lille and the French Ministry of National Education, Higher Education and Research (APAFIS#2617-2015110517317420 v5 and APAFIS#25041-2020040917227851), and under the guidelines defined by the European Union Council Directive of September 22, 2010 (2010/63/EU).

Brain Fixation

To fix the brains of mice and hamsters, animals were anesthetized with an intraperitoneal injection of Ketamine/Xylazine (80mg/100mg/Kg body weight). Mice were perfused transcardially with ice-cold NaCl 0.9% solution followed by the fixative solution. For wild type C57BL/6J mice fed standard chow or HFD, a solution of 4% paraformaldehyde in borate buffer (sodium tetraborate decahydrate pH 9.5) was used. For female mice, male NPY-GFP; POMC::Cre; tdTomato mice and hamsters, a fixative solution of PFA 4% in phosphate-buffered saline (PBS; pH 7.4) was used. Dissected brains were post-fixed for 4h in their respective fixative solutions before cryopreservation in sucrose 30% (sucrose in 0.1M phosphate buffered saline pH7.4) for 48h before cryosectioning. Hamsters were decapitated and the harvested brain immersion-fixed for 24h in 4% paraformaldehyde in phosphate buffer.

Immunohistochemistry

For triple-label immunofluorescence experiments, 30 µm-thick floating sections were rinsed 4 times in 0.1 M PBS pH 7.4 and blocked for 1 hour at room temperature in blocking solution (PBS containing 10% normal donkey serum and 0.3% Triton X-100). Sections were incubated overnight at 4°C with a mix of primary antibodies diluted in blocking solution (goat anti ACE2 1:200; rabbit anti TMPRSS2 1:1,000 and mouse anti FPR2 1:200; see Antibody table). The sections were then washed three times in 0.1M PBS and incubated for 1.5 hours at room temperature with a biotinylated donkey anti-rabbit secondary antibody to amplify the TMPRSS2 signal (1:500). The sections were then washed three times in 0.1MPBS and incubated at room temperature for 1 hour with Alexa Fluor-conjugated secondary antibodies (1:500 dilution; all purchased from Molecular Probes, Invitrogen, San Diego, CA) in blocking solution. The sections were rinsed 3 times in 0.1 M PBS. Nuclei were then counterstained by incubating the sections for 1 minute in DAPI.

Collection and processing of human tissues

Tissues were obtained in accordance with French bylaws (Good Practice Concerning the Conservation, Transformation and Transportation of Human Tissue to be Used Therapeutically, published on December 29, 1998). Permission to use human tissues was obtained from the French Agency for Biomedical Research (Agence de la Biomedecine,Saint-Denis la Plaine, France, protocol no. PFS16-002) and the Lille Neurobiobank.

Post-mortem adult human brains

Studies were undertaken on the brains of two men of 50 and 79 years of age, with no brain disease at the time of death. Dissected blocks of the adult brain containing the hypothalamus were fixed by immersion in 4% paraformaldehyde in 0.1M phosphate buffer, pH 7.4 at 4°C for 2 weeks. The tissues were cryoprotected in 30% sucrose/PBS at 4°C overnight, embedded in Tissue-Tek OCT compound (Sakura Finetek), frozen in dry ice and stored at −80°C until sectioning. For human hypothalamus immunolabeling, a citrate-buffer antigen retrieval step, 10mM Citrate in TBS-Triton 0.1% pH 6 for 30 min at 70°C, was performed on 20µm sections. After 3 washes of 5 minutes with TBS-Triton 0.1%, sections were blocked in incubation solution (10% normal donkey serum, 1mg/ml BSA in TBS-Triton 0.1% pH 7,4) for 1 hour. Blocking was followed with primary antibody incubation (see Antibody table) in incubation solution for 48h at 4°C. Primary antibodies were then rinsed out, before incubation in

fluorophore-coupled secondary antibodies or, in case of amplified immunolabeling, biotinylated secondary antibodies for 1h in TBS-Triton 0.1% at room temperature. For classic immunohistochemistry, secondary antibodies were washed and sections counterstained with DAPI (D9542, Sigma). For amplified immunohistochemistry, after secondary antibodies were rinsed, sections were incubated with VECTASTAIN® Elite ABC-HRP kit (PK-6100, Vector laboratories) following manufacturer's instructions. Sections were then incubated with biotinyl-tyramide reagent (SAT700001EA, Perkin Elmer) following manufacturer's recommendations, washed and incubated with fluorophore-coupled streptavidin (1/500 dilution in TBS-Triton 0.1%) before counterstaining with DAPI. Finally, the sections were incubated with Autofluorescence Eliminator Reagent (2160, Millipore) following manufacturer's instructions and mounted with Fluoromount™ (F4680, Sigma).

Human fetuses

Tissues were obtained in accordance with French bylaws (Good Practice Concerning the Conservation, Transformation, and Transportation of Human Tissue to Be Used Therapeutically, published on December 29, 1998). The studies on human fetal tissue were approved by the French agency for biomedical research (Agence de la Biomédecine, Saint-Denis la Plaine, France, protocol n: PFS16–002). Non-pathological human fetuses (11 and 14 gestational weeks (GW), n = 1 per developmental stage) were obtained from voluntarily terminated pregnancies after written informed consent was obtained from the parents (Gynecology Department, Jeanne de Flandre Hospital, Lille, France). Fetuses were fixed by immersion in 4% PFA at 4°C for 5 days. The tissues were then cryoprotected in PBS containing 30% sucrose at 4°C overnight, embedded in Tissue-Tek OCT compound (Sakura Finetek), frozen on dry ice, and stored at -80°C until sectioning. Frozen samples were cut serially at 20 µm intervals with a Leica CM 3050S cryostat (Leica Biosystems Nussloch GmbH) and immunolabeled, as described below and as previously described (*69*).

Embryos and fetuses were fixed by immersion in 4% paraformaldehyde in 0.1M phosphate buffer, pH 7.4 at 4°C for 2-5 days depending on sample size. The tissues were cryoprotected in 30% sucrose/PBS at 4°C overnight, embedded in Tissue-Tek OCT compound (Sakura Finetek), frozen in dry ice and stored at −80°C until sectioning. For immunolabelling, 20 µm-thick sections of entire heads at GW 11 and GW 14 were processed as follows. Slides first underwent antigen retrieval for 20 minutes in a 5mM citrate buffer heated to 90°C, then were rinsed in TBS and blocked/permeabilized for 2 hours at room temperature in TBS + 0.3% Triton + 0.25% BSA + 5% Normal Donkey Serum ("Incubation solution", ICS). Sections were then incubated with primary antibodies for two nights at 4°C in ICS. After rinses in TBS, the sections were incubated with secondary antibodies for two hours at RT in ICS, then rinsed again in TBS. Finally, nuclei were stained with DAPI (Sigma D9542, 1:5000 in TBS) for 5 minutes, and sections were rinsed before coverslipping with homemade Mowiol.

Antibody table

Antibody	Manufacturer	Reference	Dilution	Amplification
Goat anti human ACE2	R&D Systems®	AF933	1/100	Yes
Goat anti	R&D Systems®	AF3437	1/200	No

mouse ACE2				
Rabbit anti-TMPRSS2	Abcam	Ab92323	1/100-1/1000	Yes
Mouse anti-FPR2	Invitrogen	GM1D6	1/100-1/400	Yes
Chicken anti-vimentin	Millipore	AB5733	1/500	No
Goat anti-TAG1	R&D Systems®	AF4439	1/500	No
Mouse anti-FPR2	Invitrogen	GM1D6	1/400	No

Fluorescence-activated cell sorting and real-time quantitative PCR

Tat-cre infusion

A tat-cre fusion protein produced as detailed previously (*98*) was stereotaxically infused into the third ventricle (6.37 µg/2 µl at a rate of 0.2µl/ml; AP: −1.7 mm, ML: 0 mm DV: - 5.6 mm) of five isoflurane-anesthetized 4 month-old male C57Bl/6 *tdTomato*$^{loxP/+}$ reporter mice 2 weeks before experiments, as described before (*54*).

Sorting

Median eminence explants were microdissected from *tdTomato*$^{Tat\text{-}Cre}$ mice, and cell dissociated using the Papain Dissociation System (Worthington Biochemical Corporation). Fresh dissociated cells were sorted by Fluorescence-activated cell sorting (FACS) in an BD FACSAria™ III sorter.

Quantitative RT-PCR analyses

For gene expression analyses, lysates of FACS-sorted tanycytes and non-tanycytes were subjected to DNAse treatment (DNaseI EN0521, ThermoFisher) and then reverse transcribed using MultiScribe™ Reverse Transcriptase and the High-Capacity cDNA Reverse Transcription Kits (Applied Biosystems). A preamplification step was performed (TaqMan^{tm} PreAmp Master Mix Kit 4488593, Applied Biosystems) before real-time PCR. Real-time PCR was carried out on Applied Biosystems 7900HT Fast Real-Time PCR System using TaqMan® Gene Expression Assays listed below. Real-time PCR analysis were performed using the $2^{-\Delta\Delta Ct}$ method using as an internal/positive control a sample of 50pg of total RNA obtained from the mediobasal hypothalamus as extensively described previously (*99*).

RTqPCR primer table

Gapdh	Mm 99999915_g1

Ace2	Mm 01159006_m1
Fpr2	Mm 00484464_s1
Tmprss2	Mm 00443687_m1
Vimentin	Mm 01333430_m1

Methods references

91. M. C. Alessi, N. Cenac, M. Si-Tahar, B. Riteau, FPR2: A Novel Promising Target for the Treatment of Influenza. *Front Microbiol* **8**, 1719 (2017).
92. Y. Le *et al.*, Amyloid (beta)42 activates a G-protein-coupled chemoattractant receptor, FPR-like-1. *J Neurosci* **21**, RC123 (2001).
93. M. A. Panaro *et al.*, Biological role of the N-formyl peptide receptors. *Immunopharmacol Immunotoxicol* **28**, 103-127 (2006).
94. P. Langfelder, S. Horvath, WGCNA: an R package for weighted correlation network analysis. *BMC Bioinformatics* **9**, 559 (2008).
95. D. J. Stekhoven, P. Buhlmann, MissForest--non-parametric missing value imputation for mixed-type data. *Bioinformatics* **28**, 112-118 (2012).
96. M. I. Love, W. Huber, S. Anders, Moderated estimation of fold change and dispersion for RNA-seq data with DESeq2. *Genome Biol* **15**, 550 (2014).
97. G. Yu, L. G. Wang, Y. Han, Q. Y. He, clusterProfiler: an R package for comparing biological themes among gene clusters. *OMICS* **16**, 284-287 (2012).
98. M. Peitz, K. Pfannkuche, K. Rajewsky, F. Edenhofer, Ability of the hydrophobic FGF and basic TAT peptides to promote cellular uptake of recombinant Cre recombinase: a tool for efficient genetic engineering of mammalian genomes. *Proc Natl Acad Sci U S A* **99**, 4489-4494 (2002).
99. A. Messina *et al.*, A microRNA switch regulates the rise in hypothalamic GnRH production before puberty. *Nat Neurosci* **19**, 835-844 (2016).

Supplementary Figures

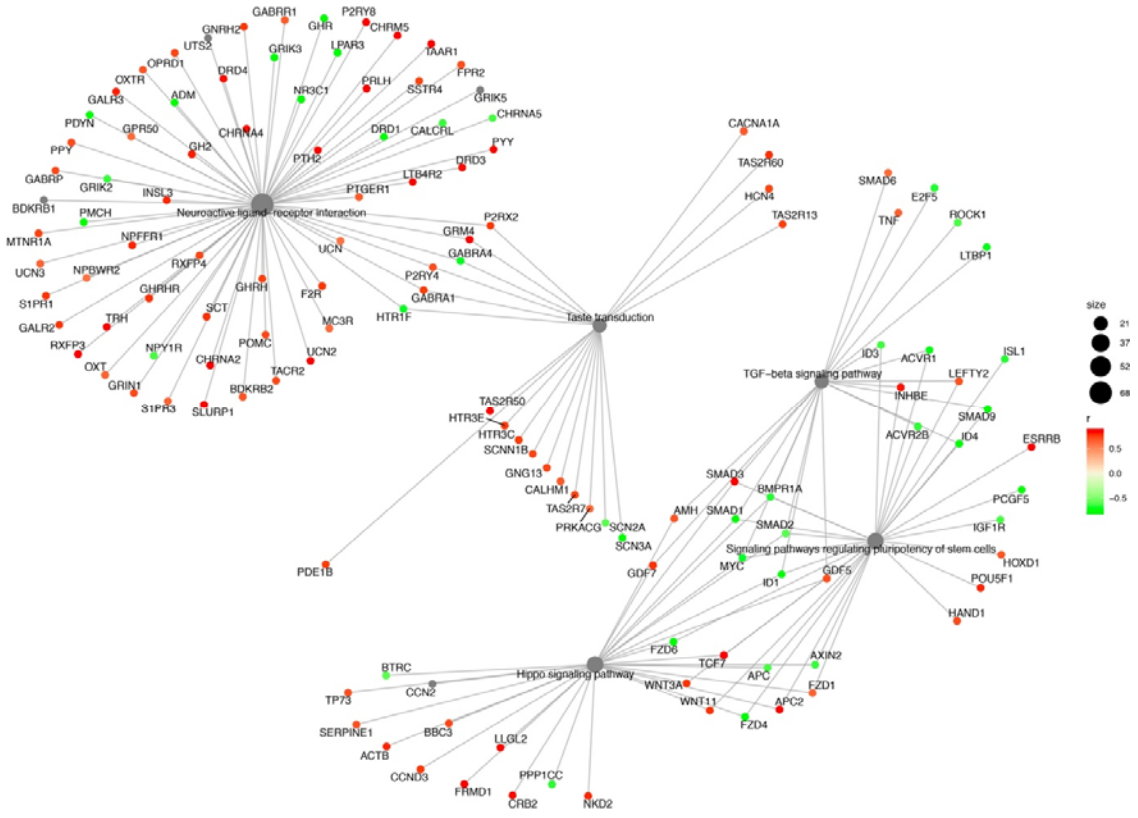

Supplementary Figure 1. Gene network of ACE2-correlated genes enriched for KEGG pathways in the insula. Pathways enriched: "neuroactive ligand-receptor interaction", "taste transduction", "TGF-beta signaling", "signaling pathways regulating pluripotency of stem cells" and "hippo signaling" pathways. Interestingly, the pathways form two subnetworks that don't appear to interact.

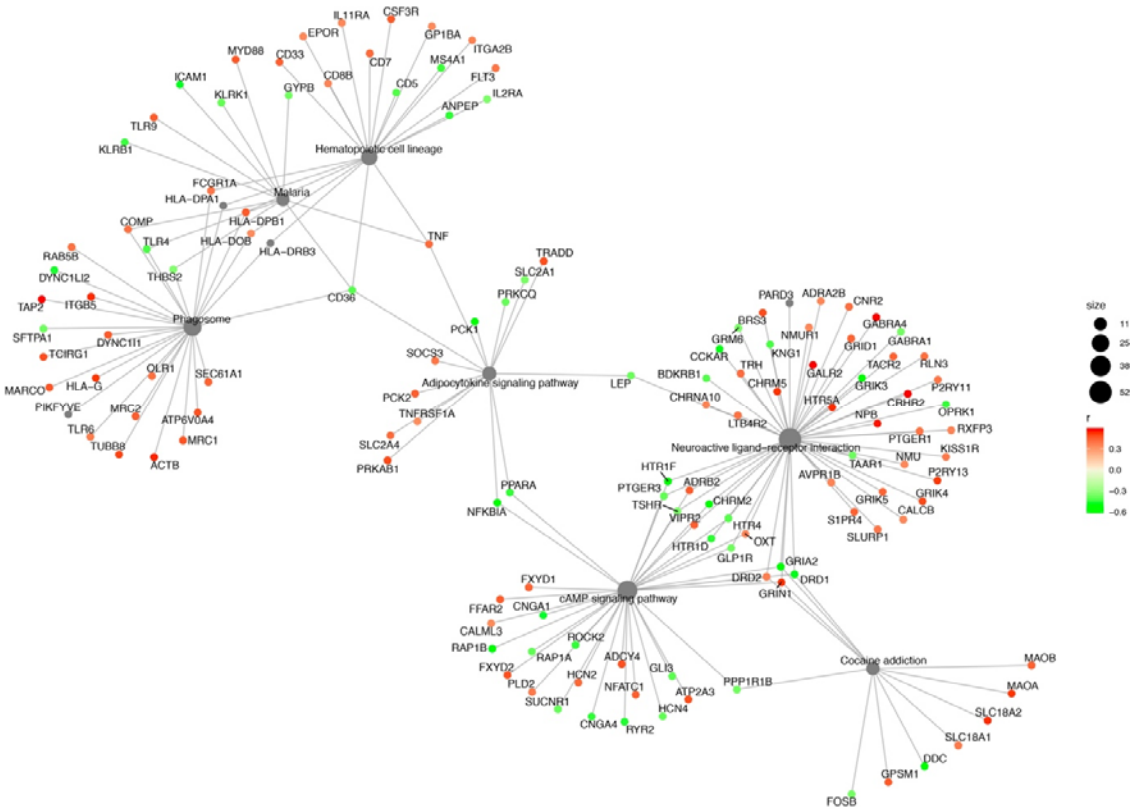

Supplementary Figure 2. Gene network of ACE2-correlated genes enriched for KEGG pathways in the amygdala. Pathways enriched: “neuroactive ligand-receptor interaction”, “hematopoietic cell lineage”, “phagosome”, cAMP signaling”, “Cocaine addiction”, “Adipocytokine signaling”, “Malaria”. The involvement of the adipocytokine signaling pathway and the phagosome pathway might have implications for metabolic risk factors and viral entry respectively.

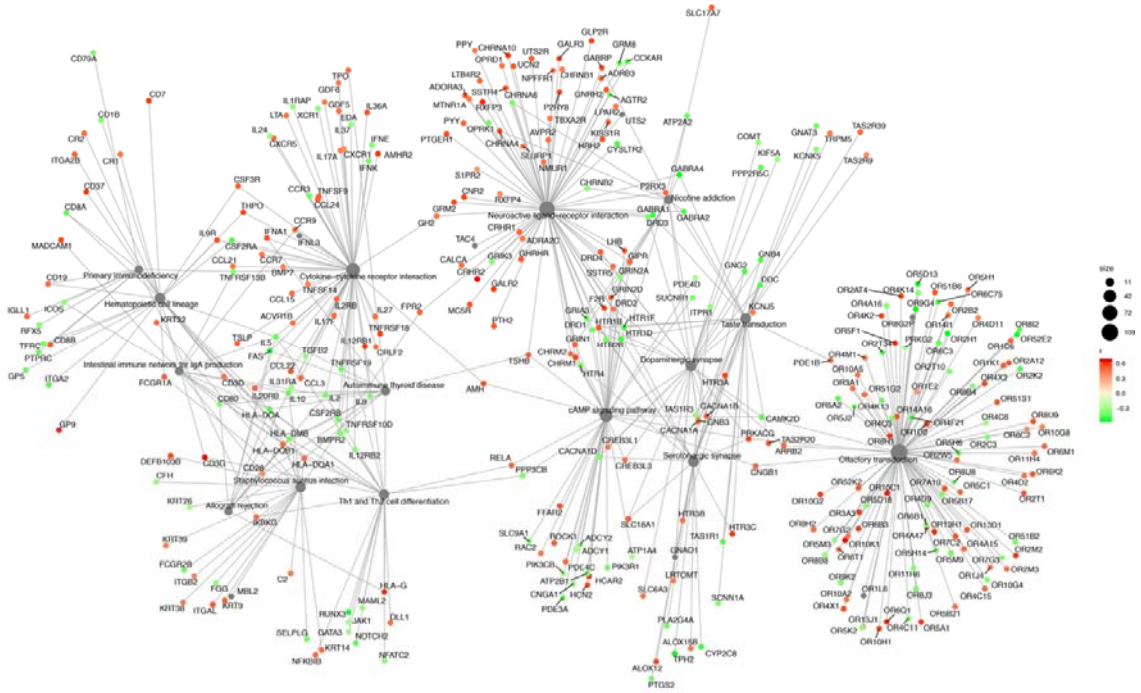

Supplementary Figure 3. Gene network of ACE2-correlated genes enriched for KEGG pathways in the hypothalamus. Out of 45 significant pathways (fdr < 0.25), the top 15 pathways of interest have been shown in the network. “olfactory transduction”, “neuroactive ligand-receptor interaction”, “taste transduction”, “nicotine addiction”, “hematopoietic cell lineage”, “cAMP signaling pathway”, “dopaminergic synapse”, “cytokine-cytokine receptor interaction”, “Th1 and Th2 cell differentiation”, “primary immunodeficiency”, “allograft rejection”, “staphylococcus aureus infection”, “autoimmune thyroid disease”, “intestinal immune network for IgA production” pathways. The extraordinarily high number of enriched and interconnected pathways with abundant correlated genes could indicate that ACE2 plays a pivotal role across multiple hypothalamic functions, and that viral alteration of ACE2 availability or function could have wide repercussions. The occurrence of a large number of olfactory and taste receptors is intriguing, even if several of the former turn out to be pseudogenes.

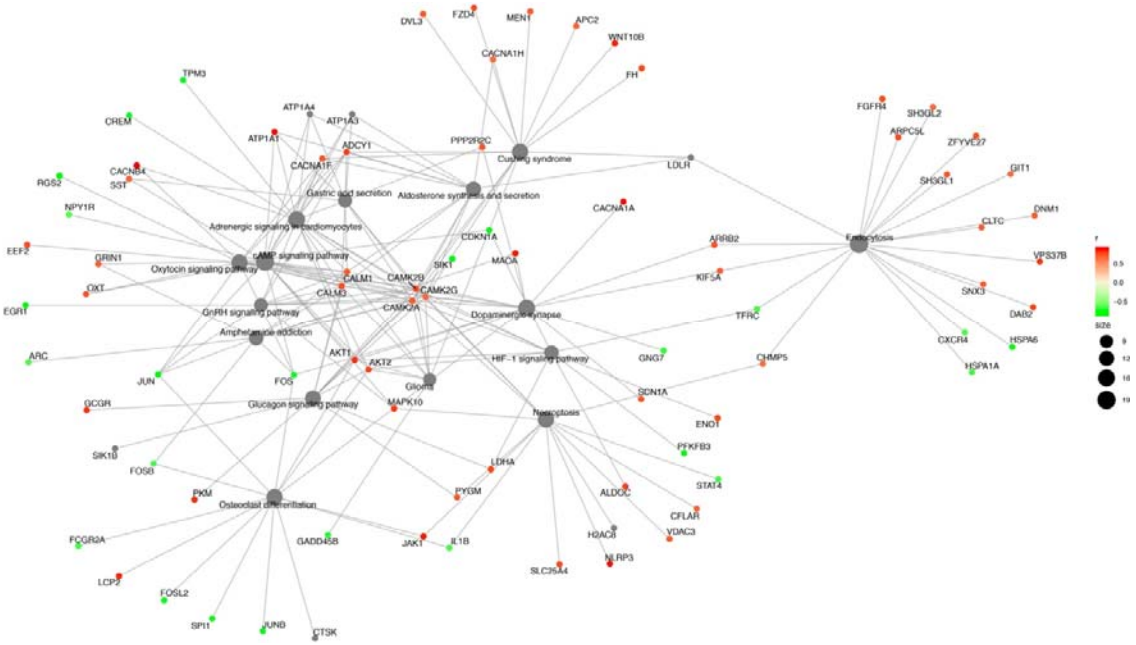

Supplementary Figure 4. Gene network of ACE2-correlated genes enriched for KEGG pathways in the parabrachial Nuclei of Pons. Out of 73 significant pathways (fdr < 0.25), the top 15 pathways of interest have been shown in the network. Pathways enriched: “dopaminergic synapse”, “amphetamine addiction”, “adrenergic signaling in cardiomyocytes”, “glucagon signaling pathway”, “aldosterone synthesis and secretion”, “osteoclast differentiation”, “cAMP signaling”, “gastric acid secretion”, “glioma”, “oxytocin signaling pathway”, “Cushing syndrome”, “endocytosis”, “GnRH signaling”, “HIF-1 signaling”, “necroptosis” pathways. In contrast to the hypothalamus, however, the number of genes per enriched pathway is fairly low, even though some genes, calmodulins and calmodulin kinases, appear to be common to a very large number of them.

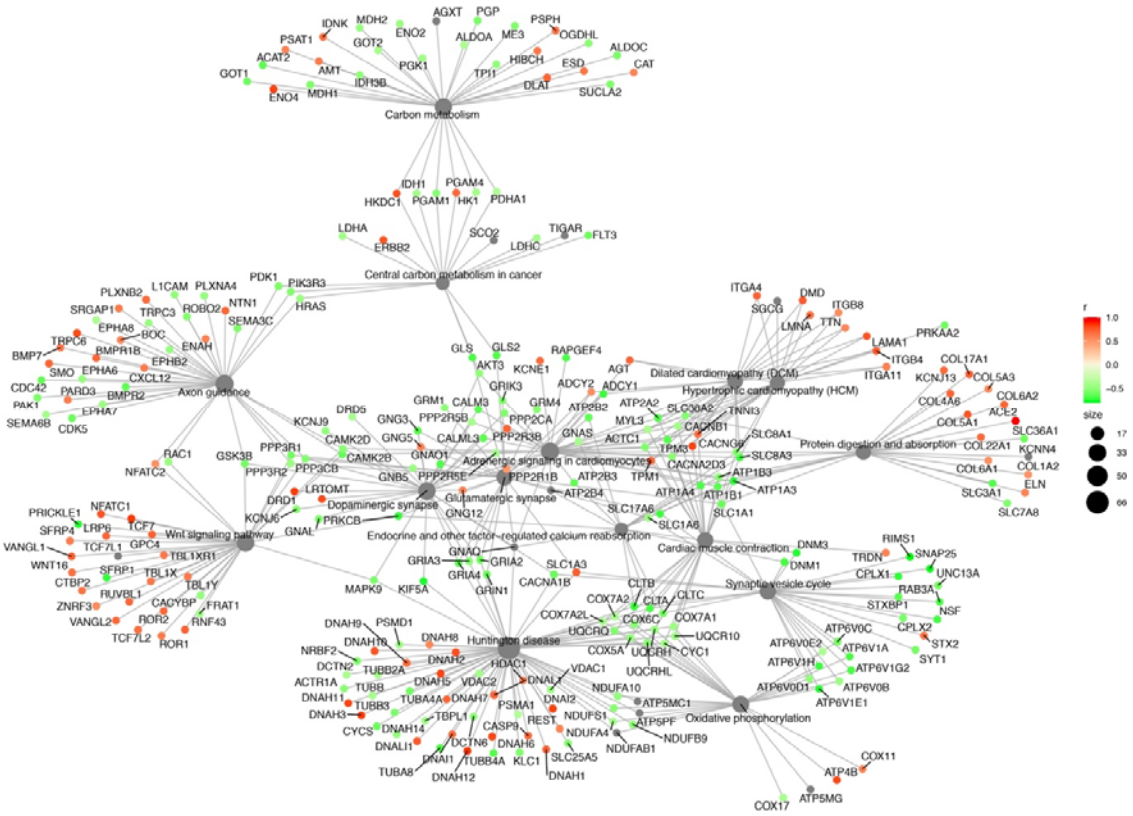

Supplementary Figure 5. Gene network of ACE2-correlated genes enriched for KEGG pathways in the myelencephalon. Out of 73 significant pathways (fdr < 0.25), the top 15 pathways of interest have been shown in the network "Huntington disease", "synaptic vesicle cycle", "cardiac muscle contraction", "carbon metabolism", "adrenergic signaling in cardiomyocytes", "dopaminergic synapse", "endocrine and other factor-regulated calcium reabsorption", "glutamatergic synapse", "dilated cardiomyopathy", "protein digestion and absorption", "oxidative phosphorylation", "hypertrophic cardiomyopathy (HCM)", "Wnt signaling pathway", "axon guidance", "central carbon metabolism in cancer" pathways. The myelencephalon, like the hypothalamus has a very large number of networks with abundant ACE2-correlated genes, in keeping with the wide range of functions that are coordinated in this region. This could contribute to the potential vulnerability of cardiorespiratory centers to infection.

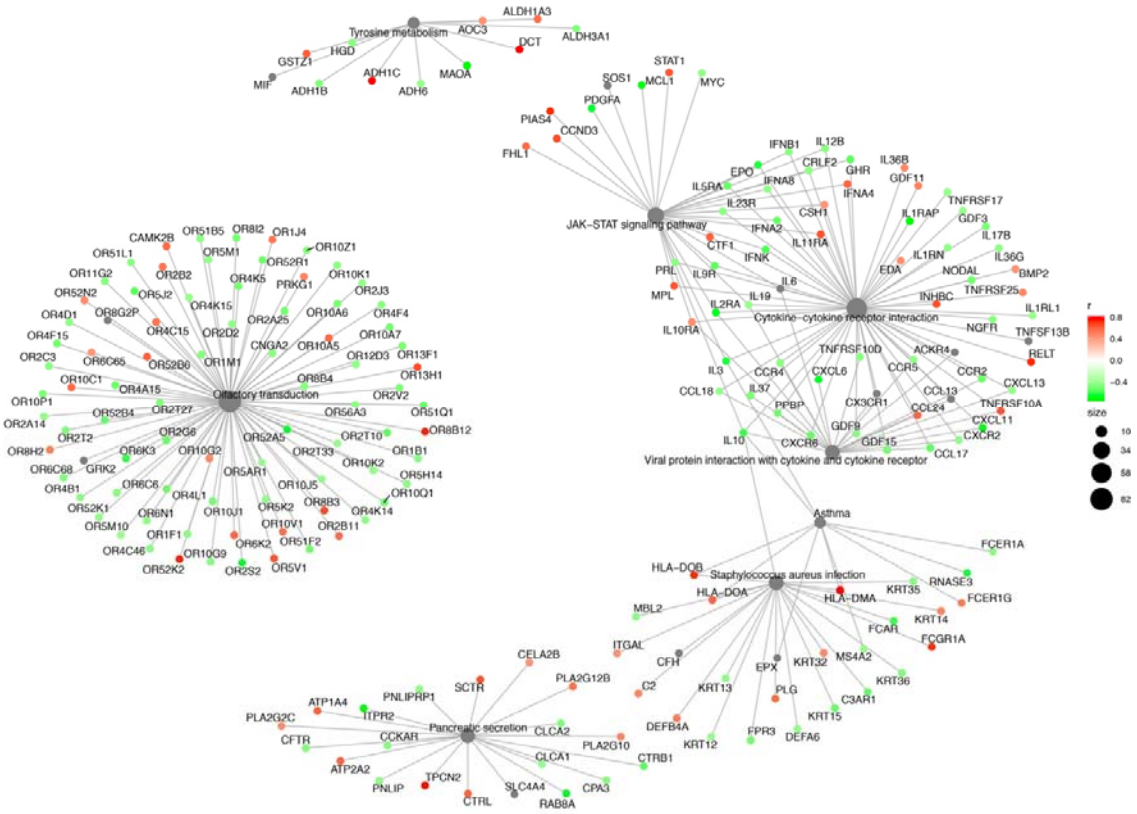

Supplementary Figure 6. Gene network of TMPRSS2-correlated genes enriched for KEGG pathways in the insula. Pathways enriched: "olfactory transduction", "tyrosine metabolism", "JAK-STAT signaling", cytokine-cytokine signaling pathway, asthma, "Staphylococcus aureus infection", "pancreatic secretion" and "viral protein interaction with cytokine and cytokine receptor" pathways. Similar to the network for ACE2-correlated genes in the insula, the TMPRSS2-correlated genes also form several subnetworks that do not interact much. Here again, the abundance of OR genes is intriguing, as is the apparent enrichment for infectious and inflammatory pathways.

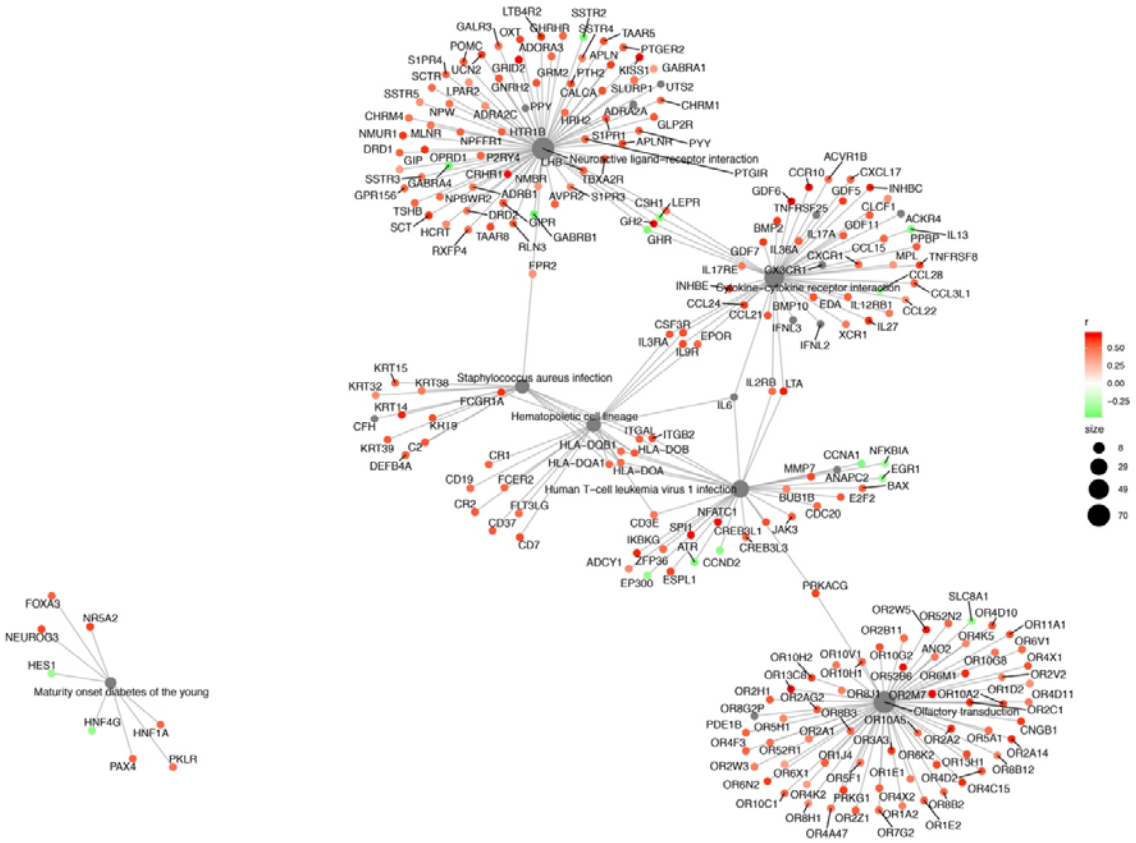

Supplementary Figure 7. Gene network of TMPRSS2-correlated genes enriched for KEGG pathways in the amygdala. Pathways enriched: "neuroactive ligand-receptor interaction", "olfactory transduction", "cytokine-cytokine receptor interaction", "maturity onset of diabetes in the young", "hematopoietic cell lineage", "human T-cell leukemia virus 1 infection", and "Staphylococcus aureus infection" pathways. As in the insula, there is a pattern of inflammatory or infectious pathways connecting other pathways.

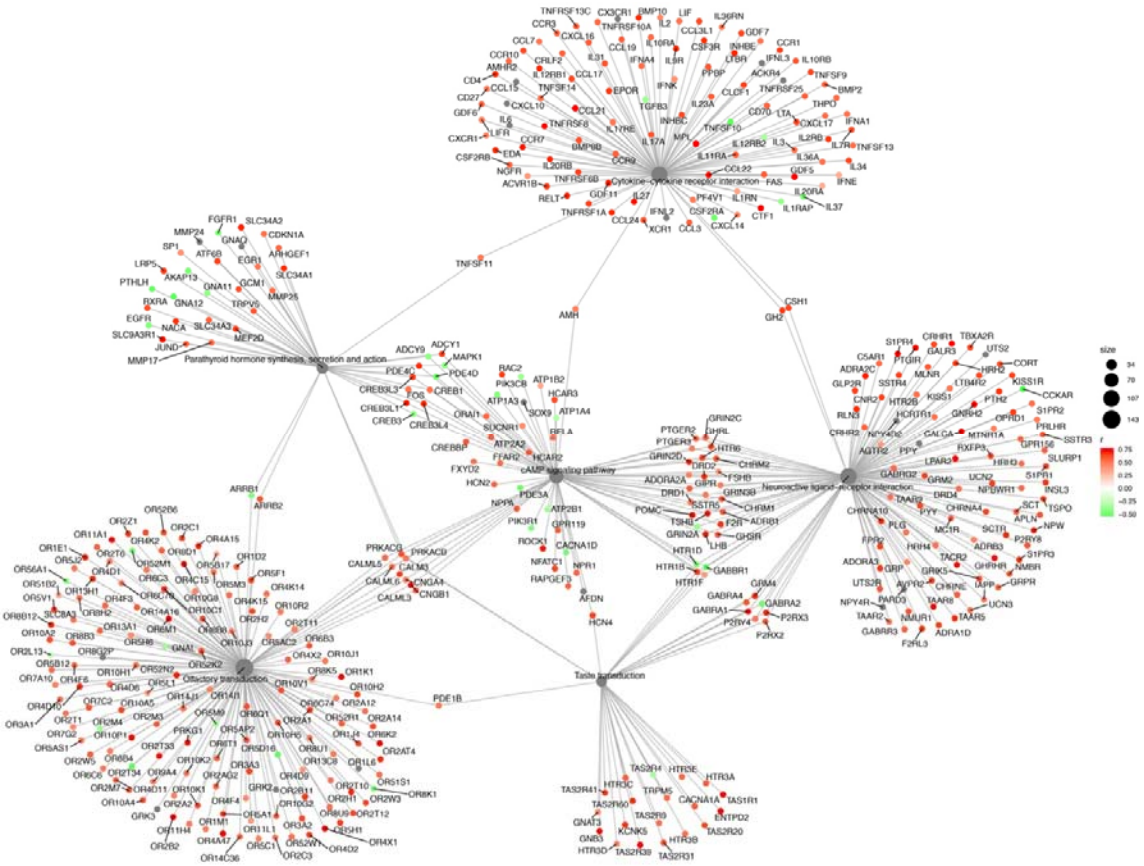

Supplementary Figure 8. Gene network of TMPRSS2-correlated genes enriched for KEGG pathways in the hypothalamus. Pathways enriched: “neuroactive ligand-receptor interaction”, “olfactory transduction”, “parathyroid hormone synthesis, secretion and action”, “taste transduction”, cAMP signaling”, pathways. The hypothalamic network for TMPRSS2-enriched genes appears less dense than that for ACE2-correlated genes. cAMP signaling appears to be a common point of interaction for diverse other networks, which do not interact much between themselves, with one or two exceptions.

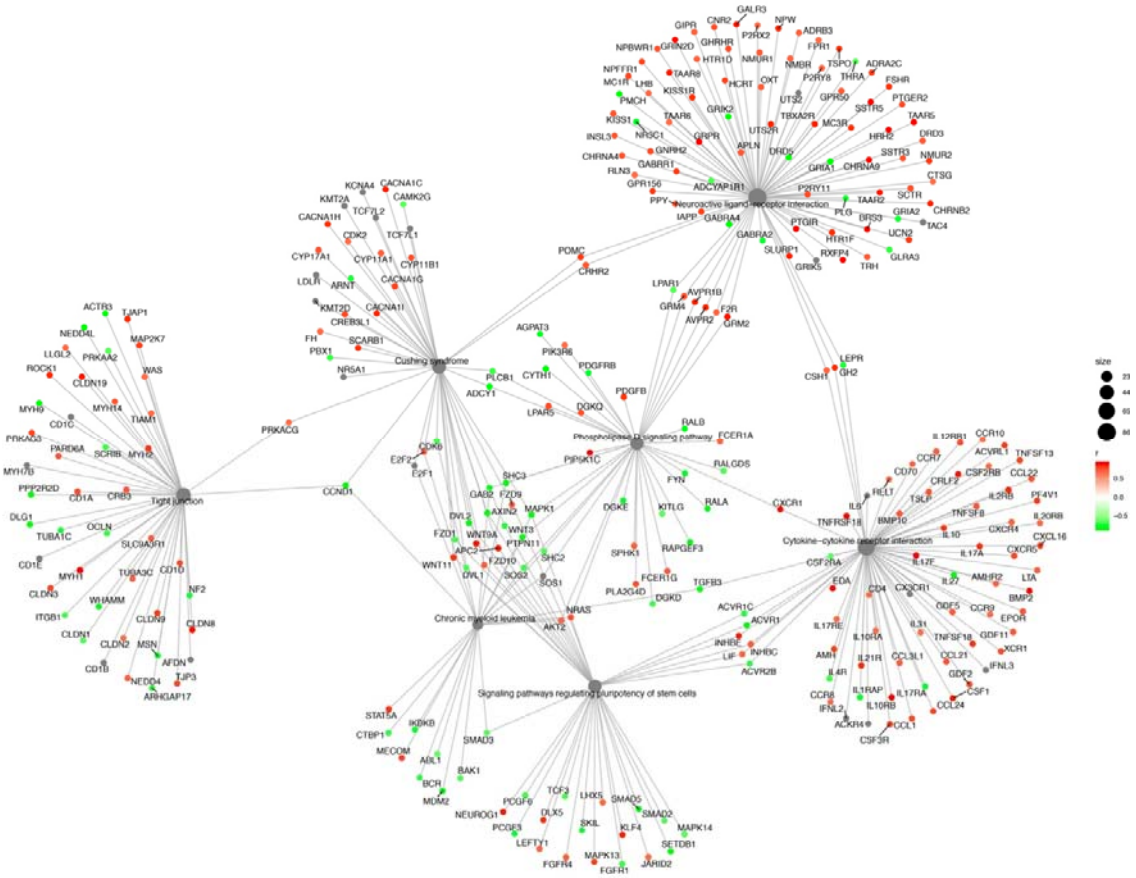

Supplementary Figure 9. Gene network of TMPRSS2-correlated genes enriched for KEGG pathways in the parabrachial nuclei of pons. Pathways enriched: “neuroactive ligand-receptor interaction”, “tight junction”, “Cushing syndrome”, “cytokine-cytokine receptor interaction”, “chronic myeloid leukemia”, “signaling pathways regulating pluripotency of stem cells”, “phospholipase D signaling” pathways.

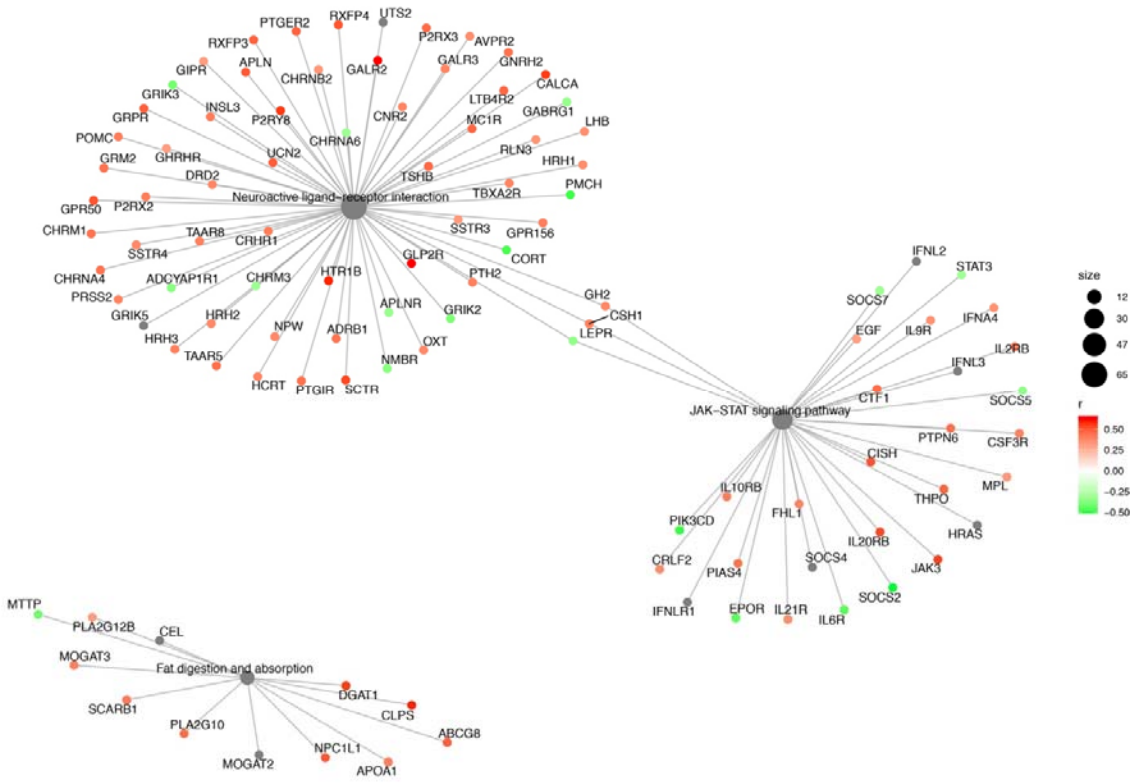

Supplementary Figure 10. Gene network of TMPRSS2-correlated genes enriched for KEGG pathways in the myelencephalon. Pathways enriched: "neuroactive ligand-receptor interaction", "JAK-STAT signaling pathway", "fat digestion and absorption". Contrary to the diversity of enriched pathways for ACE2-correlated genes, only 3 pathways were yielded for TMPRSS2-correlated genes.